Title
Beige Adipocyte Maintenance Is Regulated by Autophagy-Induced Mitochondrial Clearance

Journal
Cell Metabolism, 24(3)

ISSN
1550-4131

Authors
Altshuler-Keylin, Svetlana
Shinoda, Kosaku
Hasegawa, Yutaka
et al.

Publication Date
2016-09-01

DOI
10.1016/j.cmet.2016.08.002

Peer reviewed

Article

Cell Metabolism

Beige Adipocyte Maintenance Is Regulated by Autophagy-Induced Mitochondrial Clearance

Graphical Abstract

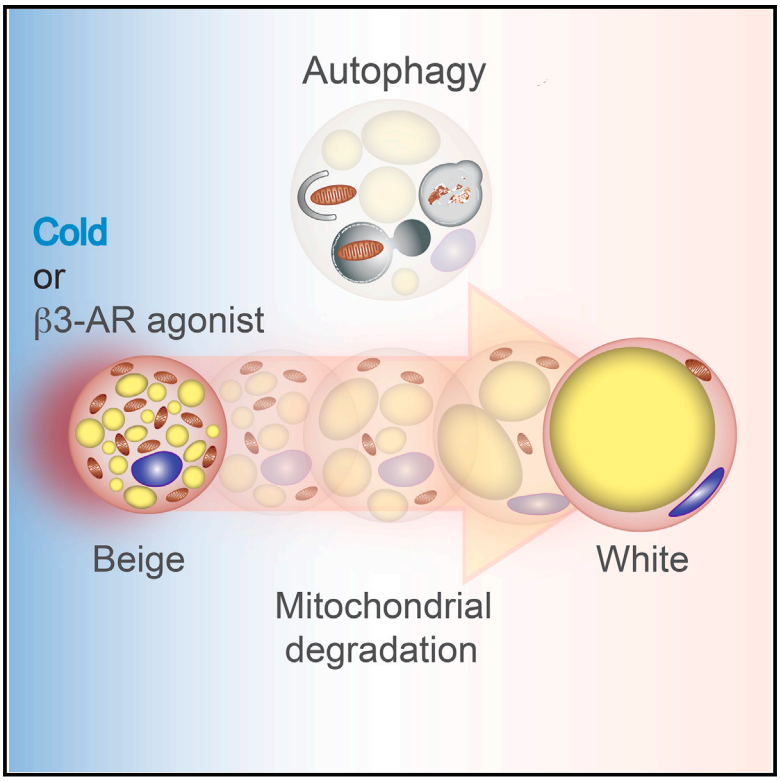

Authors

Svetlana Altshuler-Keylin, Kosaku Shinoda, Yutaka Hasegawa, ..., Rushika M. Perera, Jayanta Debnath, Shingo Kajimura

Correspondence

skajimura@diabetes.ucsf.edu

In Brief

When exposed to thermogenic stimuli, beige adipocytes transiently express UCP1 but lose that expression upon stimuli withdrawal. Altshuler-Keylin et al. investigate beige adipocyte maintenance and show that autophagy-mediated mitochondrial clearance is needed for beige-to-white adipocyte reversal. Inhibition of autophagy maintains functional beige adipocytes even after stimuli withdrawal.

Highlights

- Beige adipocytes directly acquire a "white-like" state after withdrawing stimuli
- Autophagy is activated during the beige-to-white fat transition
- Genetic and pharmacological inhibition of autophagy retains beige adipocytes
- Prolonged maintenance of beige fat ameliorates obesity and glucose intolerance

Accession Numbers

E-MTAB-3978

Altshuler-Keylin et al., 2016, Cell Metabolism *24*, 1–18
September 13, 2016
http://dx.doi.org/10.1016/j.cmet.2016.08.002

CellPress

Please cite this article in press as: Altshuler-Keylin et al., Beige Adipocyte Maintenance Is Regulated by Autophagy-Induced Mitochondrial Clearance, Cell Metabolism (2016), http://dx.doi.org/10.1016/j.cmet.2016.08.002

Cell Metabolism
Article

Beige Adipocyte Maintenance Is Regulated by Autophagy-Induced Mitochondrial Clearance

Svetlana Altshuler-Keylin,[1,2,3] Kosaku Shinoda,[1,2,3] Yutaka Hasegawa,[1,2,3] Kenji Ikeda,[1,2,3] Haemin Hong,[1,2,3] Qianqian Kang,[1,2,3] Yangyu Yang,[1,2,3] Rushika M. Perera,[4,5,6] Jayanta Debnath,[5,6] and Shingo Kajimura[1,2,3,7,*]
[1]UCSF Diabetes Center, San Francisco, CA 94143, USA
[2]Eli and Edythe Broad Center of Regeneration Medicine and Stem Cell Research, San Francisco, CA 94143, USA
[3]Department of Cell and Tissue Biology, University of California, San Francisco, San Francisco, CA 94143, USA
[4]Department of Anatomy, University of California, San Francisco, San Francisco, CA 94143, USA
[5]Department of Pathology, University of California, San Francisco, San Francisco, CA 94143, USA
[6]Helen Diller Comprehensive Cancer Center, University of California, San Francisco, San Francisco, CA 94143, USA
[7]Lead Contact
*Correspondence: skajimura@diabetes.ucsf.edu
http://dx.doi.org/10.1016/j.cmet.2016.08.002

SUMMARY

Beige adipocytes gained much attention as an alternative cellular target in anti-obesity therapy. While recent studies have identified a number of regulatory circuits that promote beige adipocyte differentiation, the molecular basis of beige adipocyte maintenance remains unknown. Here, we demonstrate that beige adipocytes progressively lose their morphological and molecular characteristics after withdrawing external stimuli and directly acquire white-like characteristics bypassing an intermediate precursor stage. The beige-to-white adipocyte transition is tightly coupled to a decrease in mitochondria, increase in autophagy, and activation of MiT/TFE transcription factor-mediated lysosome biogenesis. The autophagy pathway is crucial for mitochondrial clearance during the transition; inhibiting autophagy by uncoupled protein 1 (UCP1^{+})-adipocyte-specific deletion of *Atg5* or *Atg12* prevents beige adipocyte loss after withdrawing external stimuli, maintaining high thermogenic capacity and protecting against diet-induced obesity and insulin resistance. The present study uncovers a fundamental mechanism by which autophagy-mediated mitochondrial clearance controls beige adipocyte maintenance, thereby providing new opportunities to counteract obesity.

INTRODUCTION

Brown adipose tissue (BAT) contains thermogenic adipocytes that dissipate energy in the form of heat as an evolutionally conserved defense mechanism against hypothermia. Recent works have uncovered that humans and rodents possess two distinct forms of thermogenic adipocytes; namely classical brown adipocytes and beige (or brite) adipocytes. Brown and beige adipocytes are both competent for thermogenesis via the brown/beige-specific protein uncoupled protein 1 (UCP1) and possess similar morphological characteristics, such as multilocular lipid droplets and highly abundant mitochondria (reviewed in Kajimura et al., 2015). Nevertheless, brown and beige adipocytes arise from a distinct developmental origin. For instance, Guerra et al. (1998) and Xue et al. (2007) demonstrated that the genetic variability in controlling *Ucp1* expression was observed only in the subcutaneous white adipose tissue (WAT) of mice but not in the interscapular BAT, suggesting that brown and beige adipocytes are under different regulation and may belong to distinct developmental lineages. Furthermore, classical brown adipocytes develop prenatally from a dermomyotome population marked by *Engrailed-1*, *Myf5*, and *Pax7*, whereas beige adipocytes arise postnatally from progenitor populations in WAT expressing *Ebf2*, *Pdgfra*, and *Sca1* (Atit et al., 2006; Lee et al., 2012b; Sanchez-Gurmaches et al., 2012; Schulz et al., 2011; Seale et al., 2008; Wang et al., 2014).

Of note, adult human BAT depots from the supraclavicular and other regions contain UCP1-positve adipocytes that exhibit molecular signatures resembling murine beige adipocytes (Lidell et al., 2013; Sharp et al., 2012; Shinoda et al., 2015a; Wu et al., 2012). Importantly, the selective activation of beige adipocyte biogenesis by genetic and pharmacological approaches leads to a protection from diet-induced obesity and insulin resistance (Cederberg et al., 2001; Ohyama et al., 2016; Seale et al., 2011; Shinoda et al., 2015b). In adult human BAT, glucose uptake activity is highly induced after prolonged cold exposure, in parallel with an increase in non-shivering thermogenesis and/or an improvement in insulin sensitivity, even in subjects who had previously lacked detectable BAT depots before chronic cold exposure (Lee et al., 2014b; van der Lans et al., 2013; Yoneshiro et al., 2013). These data all support the potential significance of beige adipocytes in human obesity and diabetes and illuminate the importance of better understanding the molecular basis of beige adipocyte development and maintenance in order to pioneer future anti-obesity interventions.

An essential characteristic of beige adipocytes is its dynamic regulation of the thermogenic gene program by external stimuli. Beige adipocytes can express high levels of UCP1 in response to chronic cold exposure or β3-AR agonists, whereas classical brown adipocytes constitutively express high levels of UCP1 (Kajimura et al., 2015). Intriguingly, UCP1 expression in the

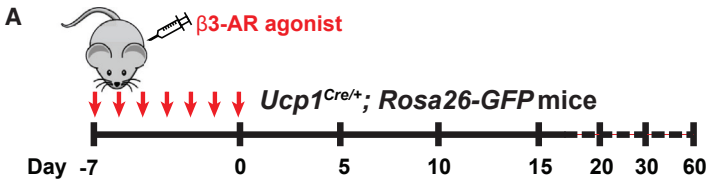

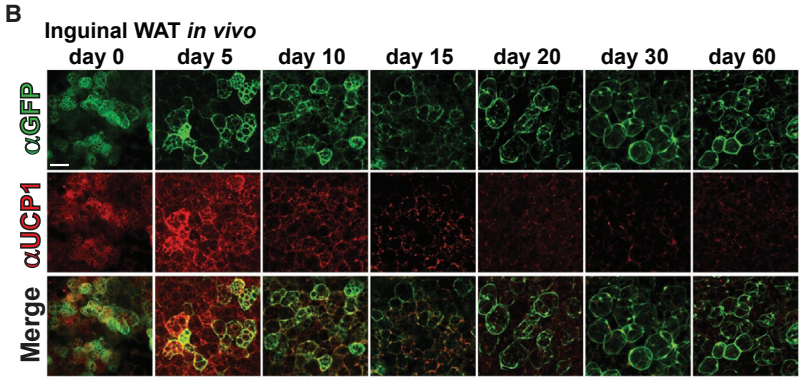

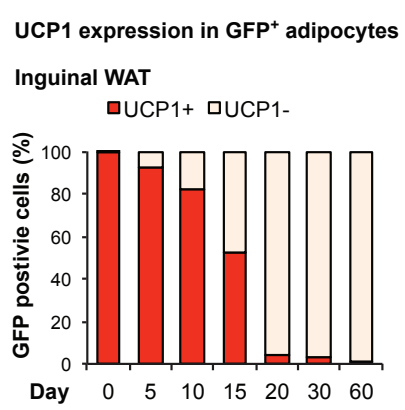

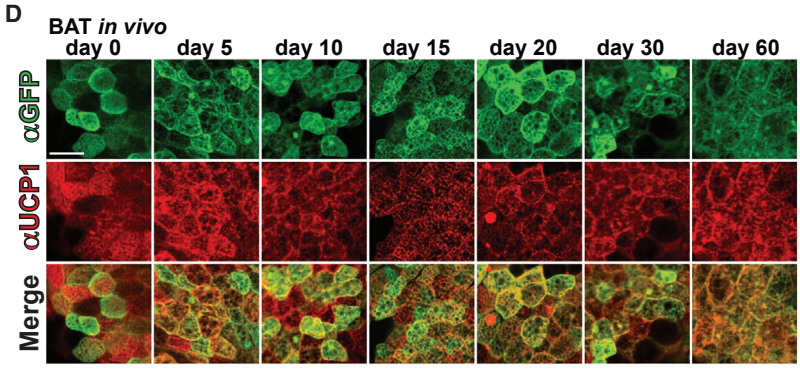

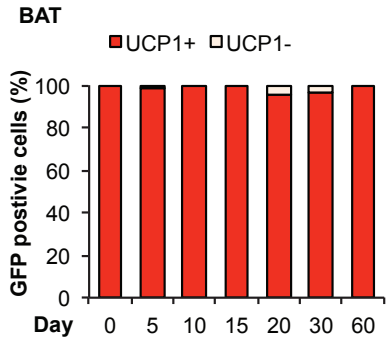

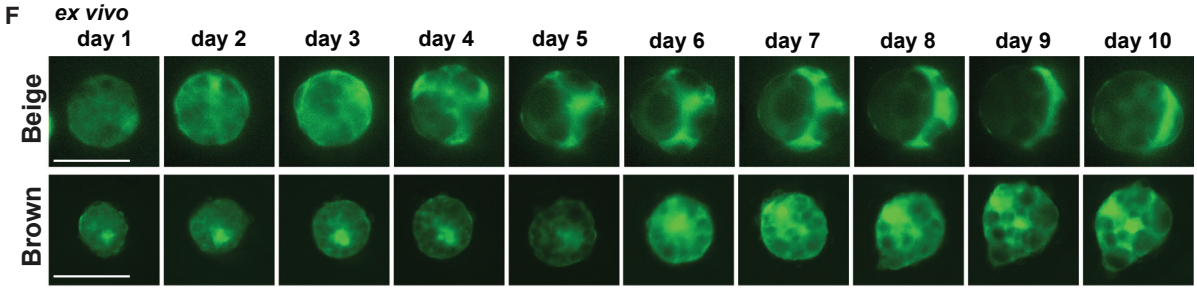

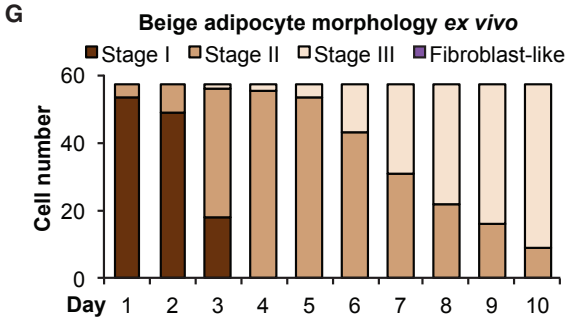

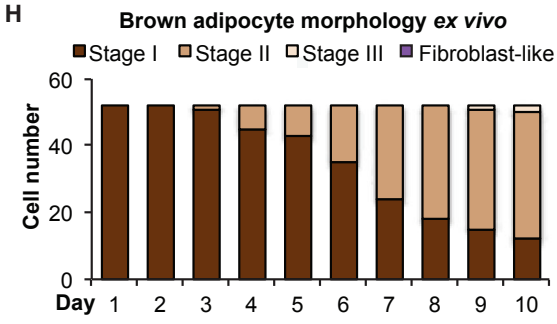

(legend on next page)

inguinal WAT became undetectable in mice within 2–3 weeks following transfer from cold environment to ambient or thermoneutral conditions (Gospodarska et al., 2015; Rosenwald et al., 2013). The cold-induced UCP1-positive beige cells became unilocular adipocytes that expressed several white adipocyte-enriched genes when re-acclimated to ambient temperature, some of which re-activate UCP1 expression in response to a subsequent bout of cold exposure (Rosenwald et al., 2013). However, the molecular mechanism of beige adipocyte maintenance remains poorly understood. Here, we demonstrate that beige adipocytes directly acquire a "white-like" phenotype after withdrawal of β3-AR agonist bypassing an intermediate precursor stage. We further show that the beige-to-white adipocyte transition is initiated by active mitochondrial clearance via autophagy. Accordingly, inhibition of autophagy by pharmacological or genetic approaches maintains thermogenically functional beige adipocytes for prolonged period of time even after withdrawal of β3-AR agonist or cold stimulus. Overall, we uncover a fundamental mechanism by which autophagy-mediated mitochondrial turnover controls beige adipocyte maintenance and whole-body energy homeostasis.

RESULTS

Beige Adipocytes Directly Acquire a White-like Phenotype

We first utilized *Ucp1*$^{Cre/+}$*;Rosa26-GFP* reporter mice and examined morphological and molecular changes of UCP1-positive beige adipocytes in vivo. Seven-day-treatment with the β3-AR agonist CL316,243 profoundly increased the number of GFP-positive beige adipocytes in the inguinal WAT (Figures 1A and 1B). These adipocytes contained multilocular lipids and co-expressed UCP1. Of note, GFP-positive beige adipocytes were undetected in the inguinal WAT of the reporter mice under thermoneutrality (30°C), but highly induced in response to the β3-AR agonist treatment (Figure S1A). Additionally, all GFP-positive adipocytes expressed endogenous UCP1 protein immediately following the β3-AR agonist treatment, further validating the experimental system (Figures 1C and S1B). Notably, 15–20 days following β3-AR agonist withdrawal, GFP-positive adipocytes exhibited near-complete loss of multilocular lipids and endogenous UCP1 expression (Figures 1B and 1C). A similar time-dependent decline in UCP1 protein expression was observed in the inguinal WAT depots after mice were acclimated from cold (6°C) to ambient temperature (Figure S1C). In contrast, classical brown adipocytes in the interscapular BAT retained multilocular lipid droplets and expressed constitutively high levels of UCP1 even 30 days after withdrawing β3-AR agonist (Figures 1D and 1E).

We postulate two potential explanations for the above results: (1) beige adipocytes de-differentiate to an intermediate precursor state and subsequently re-differentiate into unilocular adipocytes, or (2) beige adipocytes directly acquire unilocular adipocyte characteristics without going through an intermediate precursor stage. To distinguish the above two possibilities, we developed a single-cell monitoring system and tracked morphological changes of the individual beige adipocytes ex vivo for 10 days following β3-AR agonist withdrawal (Figure S2A). As shown in Figures 1F and 1G, all of the freshly isolated beige adipocytes contained multilocular lipids and began to change morphology as early as day 3, eventually becoming unilocular adipocytes. By day 10, more than 80% of the GFP-positive beige adipocytes exhibited the unilocular lipid state (stage III, Figures 1G and S2B for defining adipocyte stages). Importantly, throughout these assays, we did not observe any GFP-positive fibroblast-like cells reminiscent of precursors (Figure S2C). Consistent with the observations in vivo, the cultured beige fat progressively lost its thermogenic properties in parallel with these morphological changes (Figure S2D). In stark contrast, classical brown adipocytes retained their multilocular lipid morphology up to 10 days under the same culture conditions, although an increase in lipid size was observed in some adipocytes (Figures 1F and 1H). These data indicate that the beige adipocyte state is distinctly transient, and there is a cell-intrinsic difference between beige adipocytes and classical brown adipocytes in maintaining the multilocular lipid state following β3-AR agonist withdrawal.

Because the unilocular lipid droplet is a morphological characteristic of white adipocytes, we employed global gene expression analyses to address whether the beige adipocyte-derived unilocular adipocytes indeed acquired the molecular characteristics of white adipocytes. To this end, we performed RNA sequencing analysis of the following cell populations directly isolated from mice. First, we isolated GFP-positive adipocytes from the inguinal WAT of *Ucp1*$^{Cre/+}$*;Rosa26-GFP* reporter mice by fluorescence-activated cell sorting (FACS), which were subject

Figure 1. Beige Adipocytes Directly Acquire Morphological Characteristics of White Adipocytes after Withdrawing External Stimuli

(A) Schematic illustration of experiments to track beige adipocytes in vivo. *Ucp1*$^{Cre/+}$*;Rosa26-GFP* reporter mice were treated with the β3-AR agonist CL316,243 at 1 mg kg^{-1} for 7 consecutive days. Interscapular BAT and inguinal WAT depots were harvested for morphological and molecular analyses at the indicated time points after β3-AR agonist withdrawal.

(B) Immunohistochemistry for GFP and endogenous UCP1 expression in the inguinal WAT from *Ucp1*$^{Cre/+}$*;Rosa26-GFP* reporter mice. Inguinal WAT depots were harvested at indicated time points after β3-AR agonist withdrawal. Scale bar, 70 μm.

(C) Quantification of GFP-positive adipocytes that express endogenous UCP1 in (B). n = 150 cells or more per group.

(D) Immunohistochemistry for GFP and endogenous UCP1 expression in the interscapular BAT from *Ucp1*$^{Cre/+}$*;Rosa26-GFP* reporter mice. BAT depots were harvested at indicated time points after β3-AR agonist withdrawal. Scale bar, 40 μm.

(E) Quantification of GFP-positive adipocytes that express endogenous UCP1 in (D). n = 127 cells or more per group.

(F) Morphological changes of beige adipocytes (top) and classical brown adipocytes (bottom) using the single-cell monitoring system. GFP-positive beige or brown adipocytes were isolated from *Ucp1*$^{Cre/+}$*;Rosa26-GFP* reporter mice treated with the β3-AR agonist CL316,243 for 7 days. Morphology of the individual GFP-positive adipocytes was monitored for 10 consecutive days. Scale bar, 70 μm.

(G) Quantification of GFP-positive beige adipocytes in (F, top). Stage of each cell was estimated based on the criteria shown in Figures S2B and S2C. n = 57 cells.

(H) Quantification of GFP-positive classical brown adipocytes in (F, bottom). n = 55 cells.

See also Figure S1.

to RNA sequencing analyses at 1, 5, 10, 15, and 30 days post β3-AR agonist withdrawal (Figure 2A). As bona fide white adipocytes, we isolated GFP-positive adipocytes from the inguinal WAT of age-matched *Adiponectin*$^{Cre/+}$;*Rosa26-GFP* reporter mice. Lastly, to obtain undifferentiated adipocyte precursors, we isolated Lin$^-$/CD34$^+$/CD29$^+$/Sca1$^+$ cells from the stromal vascular fraction (SVF) of inguinal WAT of age-matched wild-type mice. As shown in Figure 2B, mRNA expression of the WAT-enriched genes, such as *Resistin*, *Wfdc21*, *Spi2*, *Ednra*, and *Psat1* (Kajimura et al., 2008), were low in beige adipocytes at day 1 and day 5 following withdrawal of β3-AR agonist, however, began to increase 10 days post β3-AR agonist withdrawal. At day 30 of withdrawal, the WAT-enriched gene expression reached levels similar to bona fide white adipocytes. In parallel to this increase, we observed a concomitant progressive decline in mRNA expression of the brown/beige-selective thermogenic genes, such as *Ucp1*, *Cidea*, *Cox8b*, and *Elovl3* (Figure 2B).

Principal component analysis (PCA) during the transition phase indicates that the gene expression profiles of the GFP-positive adipocytes at day 30 of withdrawal exhibited a molecular signature resembling white adipocytes. Most importantly, the beige adipocytes at days 5, 10, and 15 of withdrawal progressively acquired the gene signature of white adipocytes, whereas all the beige adipocytes during the transition phase were far remote from the precursors (Figure 2C). As an independent approach, hierarchical clustering based on the global gene signatures found that GFP-positive adipocytes at day 30 following β3-AR agonist withdrawal formed a cluster together with white adipocytes, which was clearly distinct from the beige adipocyte cluster at day 1 (Figure 2D). The cluster analysis demonstrated that beige adipocytes during the transition phase (days 5, 10, and 15 of withdrawal) were truly distinct from that of preadipocytes. Altogether, our data provide evidence that beige adipocytes directly acquire both the morphological and molecular characteristics resembling white adipocytes after β3-AR agonist withdrawal, bypassing an intermediate precursor stage.

The Beige-to-White Adipocyte Transition Is Coupled to Mitochondrial Clearance

To understand the mechanism by which beige-to-white adipocyte transition is regulated in vivo, we performed the Fuzzy C-Means (FCM) clustering analysis based on the obtained RNA sequencing dataset and identified nine distinct gene expression patterns during the beige-to-white adipocyte transition (Figure S3A). The most frequently observed expression profile (cluster I) contained 1,517 genes that were expressed highly in beige adipocytes immediately after the chronic treatment with β3-AR agonist (day 1) and progressively declined during the transition phase (Figure 3A). This cluster contained brown/beige fat-selective mitochondrial genes, including *Cox7a* and *Cox4i1*, and key transcriptional regulators of mitochondrial biogenesis, such as *Pgc1a*, *Pgc1b*, *Nrf1/2*, and *Tfam* (Figure 3B; Table S1).

The gene-annotation enrichment analysis found that the majority of the cluster I genes were related to mitochondrial components and function including electron transport chain and oxidative phosphorylation (Figures 3C and 3D). Furthermore, mitochondria in the inguinal WAT depots, as visualized by optical tissue clearing, were abundant immediately after the chronic treatment with β3-AR agonist, but gradually became undetected at day 15 following β3-AR agonist withdrawal or thereafter (Figure 3E, upper panel). In contrast, the interscapular BAT depots maintained high amounts of mitochondria even at day 15 or thereafter (Figure 3E, lower). Consistent with this result, protein expression of multiple mitochondrial respiratory chain components in complexes I, II, and IV, followed the pattern of UCP1 expression in inguinal WAT: highly induced upon chronic treatment with β3-AR agonist and progressively declined during the transition, reaching basal levels at 15 days post β3-AR agonist withdrawal (Figure 3F). In contrast, mitochondrial components in interscapular BAT were highly expressed and remained relatively unchanged even after β3-AR agonist withdrawal (Figure 3G). This is likely due to active mitochondrial biogenesis, because transcriptional regulators of mitochondrial biogenesis, such as *Pgc1a* and *Tfam*, persist at high levels in the BAT following β3-AR agonist withdrawal (Figure S3B). These data indicate that the beige-to-white adipocyte transition in inguinal WAT is tightly coupled to a progressive decline in mitochondria.

Activation of Autophagy during the Beige-to-White Adipocyte Transition

Mitochondrial content is tightly maintained by the balance between mitochondrial biogenesis and clearance. In fact, transcriptional regulators of mitochondrial biogenesis, including *Pgc1a*, *Nrf1/2*, and *Tfam*, were quickly downregulated in the early phase of beige-to-white adipocyte transition (Figure 3B). On the other hand, mitochondrial degradation is mediated by a form of autophagy, termed mitophagy (Klionsky et al., 2016). Notably, our RNA sequencing analysis indicated an upregulation of numerous core components of the autophagy machinery, including *Atg4b*, *Atg12*, and *Atg16*, during the beige-to-white adipocyte transition (Figure 4A). In addition, many of the autophagy-related components and lysosomal enzymes, including *Cts* genes, *Arsg*, and *Naga* (Perera et al., 2015), were highly increased during the transition and remained high in unilocular adipocytes. The gene enrichments in the autophagy pathway and the lysosome pathway were highly significant, as kurtosis (an indicator of peakedness of a distribution) in both pathways was platykurtic (K = −0.03 and −0.24, respectively), whereas that in randomly selected genes exhibited normal distribution (mesokurtic, K = 1.07) (Figure 4B). Importantly, electron microscopic (EM) analyses of beige adipocytes during the transition phase identified a number of autophagic vacuoles containing remnant mitochondrial cristae structures (Figures 4C and S4A–S4F), morphologically consistent with the induction of mitophagy (Klionsky et al., 2016).

Based on these results, we sought to confirm whether autophagy was indeed occurring in vivo during the beige-to-white adipocyte transition. To this end, we used *GFP-LC3* mice to assess the levels of punctate LC3, an indicator of autophagosome formation (Mizushima et al., 2004). We observed that these GFP-LC3 puncta were frequently co-localized with mitochondria, consistent with our findings by EM and suggestive of active mitophagy (Figure 4D). To examine whether autophagy activity is regulated during the beige-to-white adipocyte transition, we performed the following experiments. First, we quantified the number of GFP-LC3 puncta in beige adipocytes during the transition; we observed a significantly lower number of GFP-LC3 puncta in beige adipocytes residing in the inguinal WAT of mice chronically

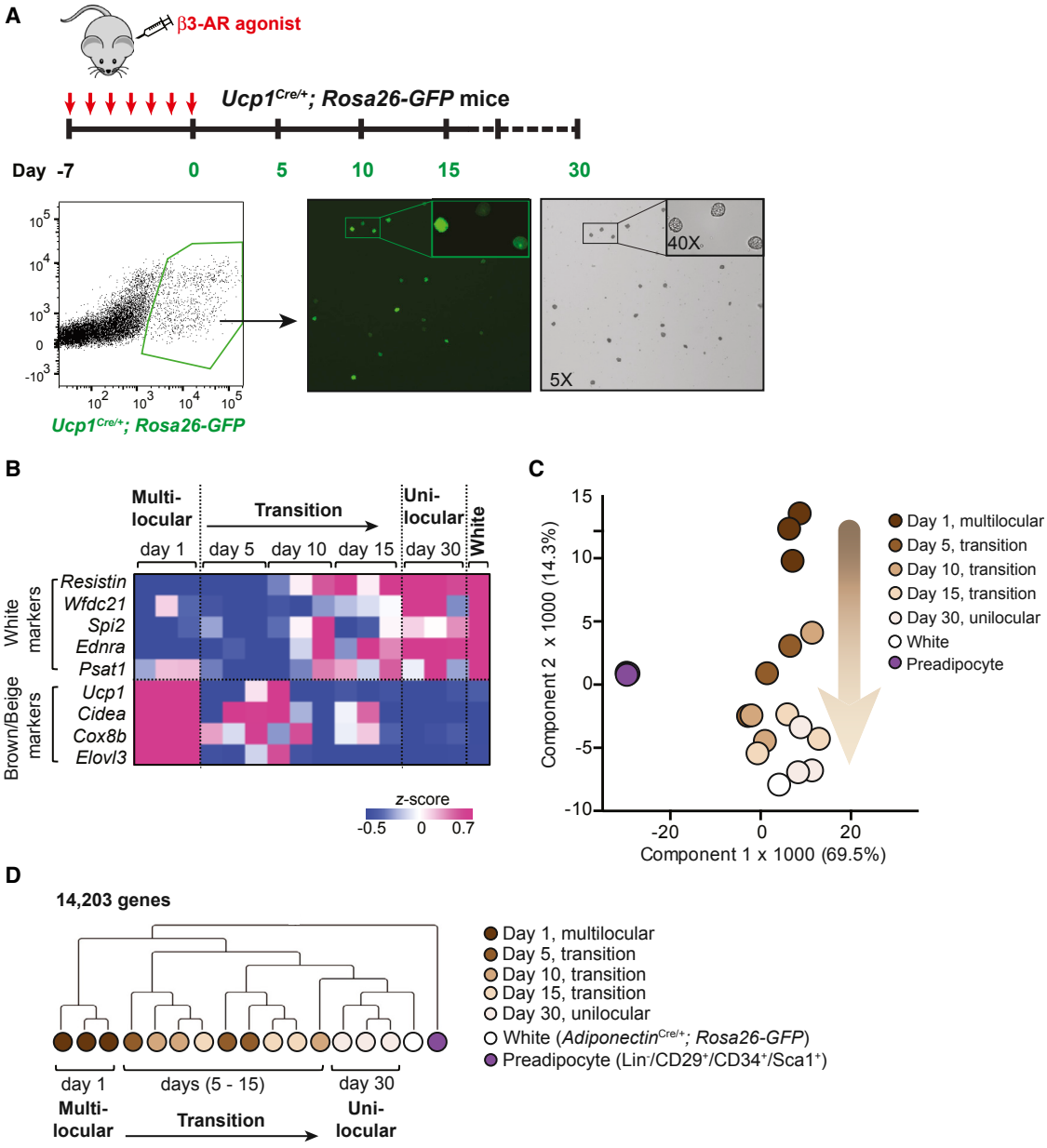

Figure 2. Beige Adipocytes Directly Acquire Molecular Characteristics of White Adipocytes after Withdrawing External Stimuli

(A) Top: schematic illustration for isolating GFP-positive adipocytes by FACS at the indicated time points in the inguinal WAT of *Ucp1*$^{Cre/+}$;*Rosa26-GFP* reporter mice. Bottom: gating strategy for isolating GFP-positive adipocytes. GFP positive adipocytes were visualized after sorting at day 1 of β3-AR agonist withdrawal. Note that all the FACS-isolated cells (bright-field) express GFP and that all of the GFP positive cells from day 1 of β3-AR agonist withdrawal contained multilocular lipids.

(B) Expression profiles of the WAT-enriched genes and brown/beige fat-enriched genes in the GFP-positive FACS-isolated beige adipocytes at indicated time points after β3-AR agonist withdrawal as described in (A). The color scale shows *Z* scored FPKM representing the mRNA level of each gene in blue (low expression)-white-red (high expression) scheme. Gene expression in the white adipocytes FACS-isolated from the inguinal fat pad of age-matched *Adiponectin*$^{Cre/+}$;*Rosa26-GFP* reporter mice is shown in the right column.

(C) Principal component analysis (PCA) of transcriptome in FACS-isolated beige adipocytes (*Ucp1*$^{Cre/+}$;*Rosa26-GFP*), FACS-isolated white adipocytes (*Adiponectin*$^{Cre/+}$;*Rosa26-GFP*), and undifferentiated adipocyte precursors (Lin$^-$/CD34$^+$/CD29$^+$/Sca1$^+$) from the SV fraction of inguinal WAT of age-matched wild-type mice. The number in parentheses represents the proportion of data variance explained by each PC.

(D) Hierarchical clustering of beige adipocytes, white adipocytes, and undifferentiated adipocyte precursors. The clustering was generated based on the RNA sequencing data of GFP-positive beige adipocytes at day 1 of β3-AR agonist withdrawal (multi-locular state), at days 5, 10, and 15 of withdrawal (transition phase), and at day 30 of withdrawal (unilocular state). White adipocytes and undifferentiated precursors are shown in white and purple circles, respectively. The clustering was visualized by MeV. The horizontal distance represents similarities among each cluster.

See also Figure S2.

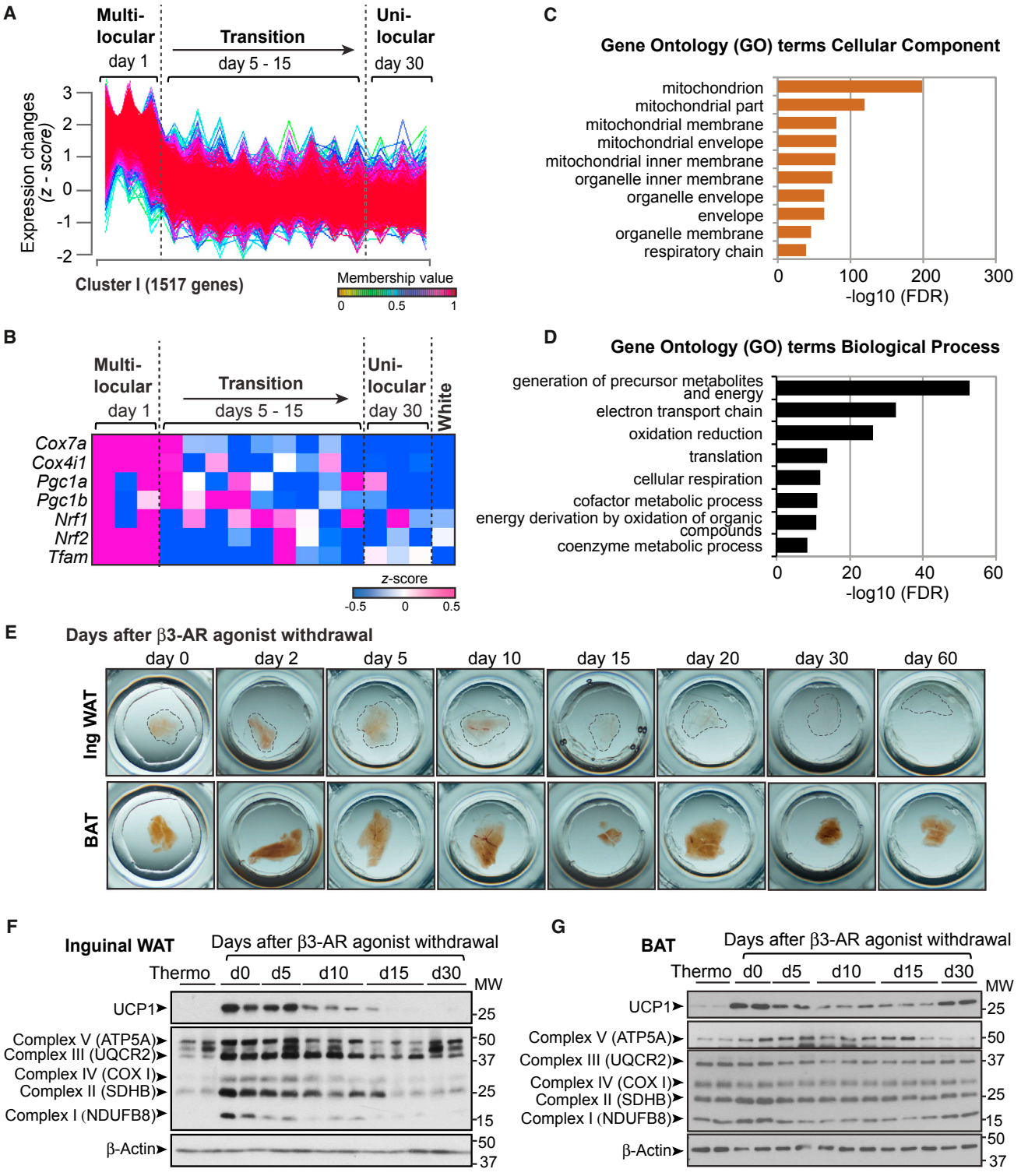

Figure 3. Beige-to-White Adipocyte Transition Is Accompanied by Mitochondrial Clearance

(A) Gene expression profile of 1,517 genes that belongs to Cluster I during the beige-to-white adipocyte transition. y axis represents expression changes in the expression level (*Z* scored FPKM) of each gene. Gene expression profiles of other clusters are shown in Figure S3A.

(B) Expression profiles of brown/beige-enriched mitochondrial genes (*Cox7a* and *Cox4i1*) and key transcriptional regulators of mitochondrial biogenesis (*Pgc1a*, *Pgc1b*, *Nrf1/2*, and *Tfam*) in the GFP-positive adipocytes at indicated time points after β3-AR agonist withdrawal. The color scale shows *Z* scored FPKM representing the mRNA level of each gene in blue (low expression)-white-red (high expression) scheme. Gene expression in the white adipocytes isolated from *Adiponectin*$^{Cre/+}$;*Rosa26-GFP* reporter mice is shown in the right column. n = 3 for each time point of beige-to-white transition.

(legend continued on next page)

treated with the β3-AR agonist (day 0), as compared to adipocytes in the inguinal WAT of saline-treated GFP-LC3 mice (Figures 4D and 4E). The number of GFP-LC3 puncta was significantly increased at 5 days post β3-AR agonist withdrawal and remained high 15 days following withdrawal. Second, we employed flow cytometric quantification of GFP-LC3 fluorescence levels to assess autophagic flux, as previously described (Shvets et al., 2008) (Figure S4G). We observed a clear increase in GFP-LC3 levels in day 0 beige adipocytes treated with β3-AR agonist, as compared to white adipocytes from the saline-treated mice (Figure 4F). After β3-AR agonist withdrawal, GFP-LC3 levels in beige adipocytes gradually decreased, indicative of increased autophagic flux in vivo, eventually reaching the levels seen in white adipocytes from the saline-treated mice (days 5, 15, and 30 in Figure 4F). Lastly, we found that LC3-II was reduced in the beige adipocytes at day 0, which correlated with increased protein accumulation of the autophagy cargo receptors, NBR1 and p62/SQSTM1 (Figure 4G), both of which are selectively degraded via autophagy (Klionsky et al., 2016). These markers subsequently returned to the basal levels observed in the saline-treated WAT at 30 days after β3-AR agonist withdrawal (Figure 4G). Notably, LC3-II was reduced upon forskolin treatment in beige adipocytes in the presence and absence of the lysosomal inhibitor Bafilomycin A1 (BafA1) (Figure S4H). These data collectively suggest that autophagy activity is low in beige adipocytes, whereas it is transiently re-activated during the beige-to-white adipocyte transition following β3-AR agonist withdrawal.

Autophagy in Beige Adipocytes Is Regulated by the cAMP-PKA Pathway and the MITF Transcription Factor

Next, we aimed to identify the upstream regulatory circuits controlling autophagy during the beige-to-white adipocyte transition. The Database for Annotation, Visualization and Integrated Discovery (DAVID) analysis identified a "lysosome" gene ontology signature ($p = 7.0 \times 10^{-4}$ after Bonferroni correction) as the top biological pathway that was transiently elevated during the transition phase (Figure 5A). Recent studies have highlighted the importance of transcriptional regulation in autophagosome formation and lysosome biogenesis by the MiT/TFE family of transcription factors (MITF, TFEB, and TFE3) (Perera et al., 2015; Sardiello et al., 2009; Settembre et al., 2011) as well as by other transcriptional regulators, such as FOXK (Bowman et al., 2014), FOXO3 (Warr et al., 2013), FXR/CREB (Lee et al., 2014a; Seok et al., 2014), and ZKSCAN3 (Chauhan et al., 2013). Therefore, we employed the Hypergeometric Optimization of Motif EnRichment analysis (HOMER) (Heinz et al., 2010) to identify conserved transcription factor binding motifs on the regulatory regions of the autophagy genes that were activated during the beige-to-white adipocyte transition. We found that the most enriched sequence motif from this analysis was the "CLEAR" consensus sequence (5′-GTCACGTGAC-3′) to which the MiT/TFE family of transcription factors (MITF, TFEB, and TEF3) are known to bind ($p = 1.0 \times 10^{-12}$) (Figure 5B) (Sardiello et al., 2009; Settembre et al., 2011). The HOMER analysis also identified a FOXO-binding motif, however, this was much less enriched than the CLEAR binding element ($p = 1.0 \times 10^{-2}$) (Figure S5A). In a completely independent unbiased analysis from our previous RNA sequencing dataset (Shinoda et al., 2015a), we found that 91.6% (121 out of 132 genes) of the autophagy-related lysosome genes (Perera et al., 2015) were significantly downregulated in the inguinal WAT by chronic cold exposure for 5 days (Figure 5C). Importantly, 78.8% of the autophagy-related lysosome genes (104 out of 132 genes) were decreased both by chronic cold exposure and chronic administration of β3-AR agonist (Figure 5D), indicating that cold exposure and β3-AR agonist similarly repress lysosome biogenesis in vivo. The HOMER-based motif analysis on the cold/β3-AR agonist-regulated lysosome gene signature similarly identified the CLEAR sequence as the most enriched transcription factor-binding site (not shown).

Of the three MiT/TFE family transcription factors, we found that *Mitf* expression was significantly induced during the initiation of beige-to-white adipocyte transition. In contrast, expression of *Tfeb* and *Tef3* remained unchanged during the transition (Figure 5E). Notably, previous studies (Perera et al., 2015; Sardiello et al., 2009; Settembre et al., 2011) have shown that all the autophagy-related lysosome genes, including *Cts* genes (Cathepsin gene family), and several autophagy components activated during the beige-to-white adipocyte transition (as listed in Figure 4A) are direct targets of MiT/TFE transcription factors.

We further investigated the extent to which MITF and its downstream autophagy-lysosome signature are regulated by β-AR signaling in beige adipocytes. Protein kinase A (PKA) is well known to negatively regulate autophagy either by phosphorylation of LC3 or by activating mTORC1 that inhibits autophagy (He and Klionsky, 2009). On the other hand, activation of PKA in response to stimulation of β-AR positively promotes beige adipocyte development through transcriptional activation of the thermogenic gene program and mTORC1 (Liu et al., 2016). Thus, we hypothesized that activation of the PKA pathway via β-AR stimulation represses the autophagy network in beige adipocytes, whereas removal of the β-AR agonist leads to autophagy activation during the beige-to-white adipocyte transition. Accordingly, when differentiated beige adipocytes in culture were treated with forskolin (cAMP), *Mitf* expression was significantly decreased (Figure 5F). Co-treatment with the PKA inhibitor, H89, largely alleviated both cAMP-mediated repression of *Mitf* levels (Figure 5F) and LC3-II turnover (Figure S4H), thereby corroborating a critical role of the PKA pathway for inhibiting autophagy in beige adipocytes. Consistent with the modest enrichment of a FOXO3 binding motif, *Foxo3* expression was

(C) GO analysis (cellular component) of the genes in Cluster I (GO FAT).
(D) GO analysis (biological process) of the genes in Cluster I (GO FAT).
(E) Inguinal WAT and BAT depots (3–5 mm diameter) at indicated time points after β3-AR agonist withdrawal were fixed in 4% PFA and cleared for optical imaging.
(F) Immunoblotting for UCP1 and the indicated mitochondrial complex components in the inguinal WAT depots of wild-type mice under thermoneutrality and at indicated time points (days 0–30) following β3-AR agonist withdrawal. β-actin was used as a loading control. Molecular weight (MW) is shown on the right.
(G) Immunoblotting for UCP1 and the indicated mitochondrial complex components in the interscapular BAT depots of wild-type mice in (F).
See also Table S1.

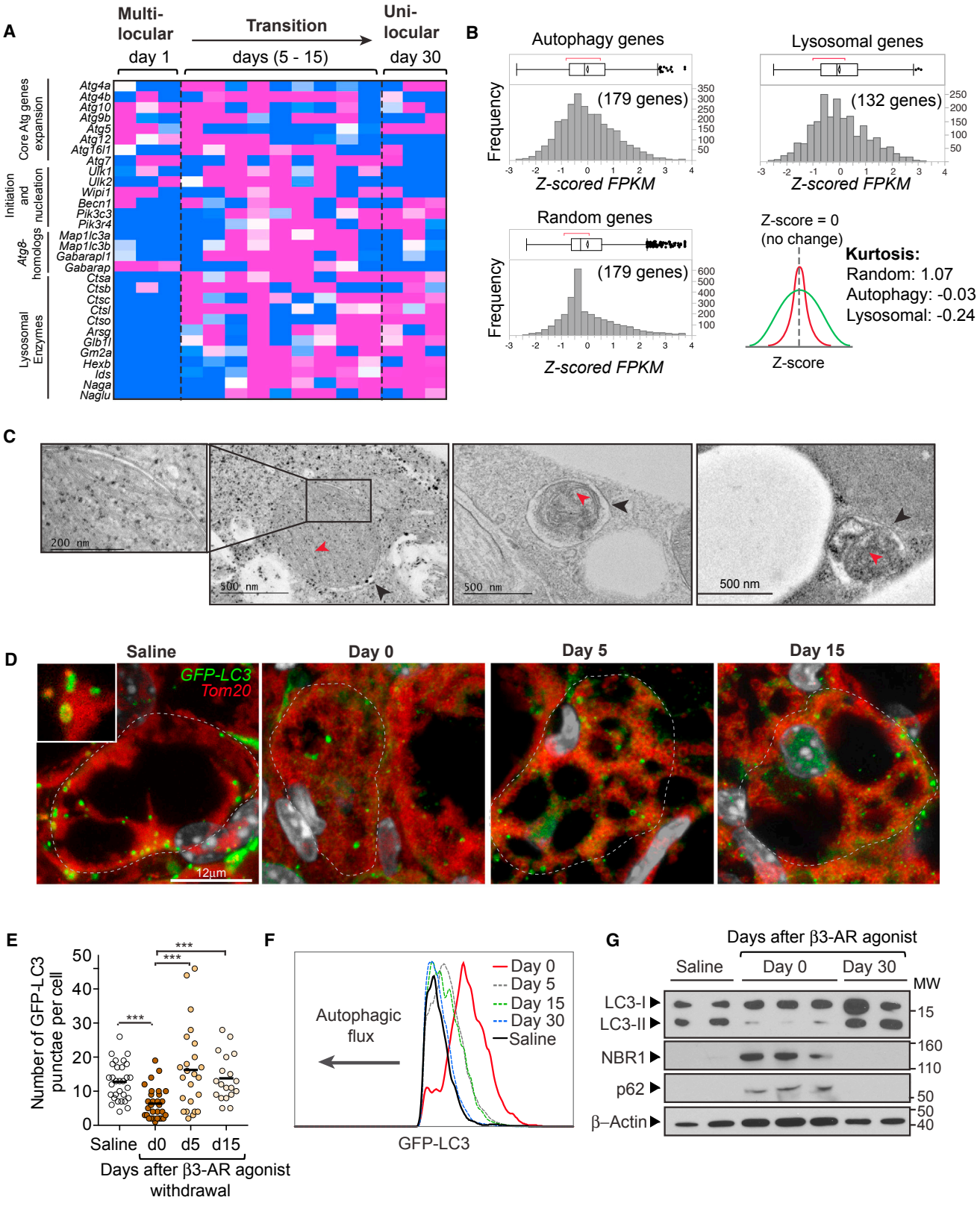

Figure 4. Activation of Autophagy during the Beige-to-White Adipocyte Transition

(A) Expression profile of the autophagy-related genes during the beige-to-white adipocyte transition. The color scale shows *Z* scored FPKM representing the mRNA level of each gene in blue (low expression)-white-red (high expression) scheme. n = 3 for each time point.

(legend continued on next page)

transiently activated during the beige-to-white adipocyte transition and repressed by cAMP through the PKA pathway (Figures S5B and S5C). Importantly, the cAMP-PKA-mediated repression of *Mitf* and *Foxo3* was accompanied by a transcriptional repression of their target genes encoding components of autophagy machinery, such as *Wipi*, *Bnip*, *Bnip3l*, and autophagy-related lysosome genes (Figure 5G). Of note, the cAMP pathway was able to repress *Mitf* and autophagy-related lysosome gene expression in beige adipocytes even under starvation conditions, suggesting that the cAMP-mediated repression on autophagy occurs independently of nutritional cues (Figures 5H and 5I). Taken together, these results indicate that autophagy in beige adipocytes is regulated by the cAMP-PKA pathway and the MITF transcription factor.

Autophagy-Mediated Mitochondrial Clearance Controls Beige Adipocyte Maintenance

The results above motivate the hypothesis that autophagy-induced mitochondrial clearance is functionally required for beige adipocyte maintenance. Previous studies showed that genetic deletion of *Atg7* via *Fabp4-Cre* resulted in increased beige adipocyte differentiation in vivo (Singh et al., 2009; Zhang et al., 2009). However, as *Fabp4-Cre* is active in brown, beige, and white adipocytes as well as some non-adipose tissues including skeletal muscle (Mullican et al., 2013), and because *Atg7* deletion in skeletal muscle promotes beige adipocyte differentiation (Kim et al., 2013), the *Fabp4-Cre* model is not suitable to test the specific requirement of autophagy for "maintenance" of beige adipocytes. Thus, we used *Ucp1-Cre* mice (Kong et al., 2014) to generate mature brown/beige adipocyte-specific deletion of *Atg5* or *Atg12*, two core autophagy regulators that are essential for the early steps of autophagosome formation (Mizushima and Komatsu, 2011). Although no *Cre* line currently exists to specifically target mature beige adipocytes without affecting classical brown adipocytes, this model allows us to test the requirement of autophagy for maintenance of newly developed beige adipocytes in response to cold or β3-AR agonist, given the specific expression of *Ucp1* in mature brown and beige adipocytes.

The ATG12-ATG5 complex was deleted selectively in the BAT but not in the liver, using two systems: $Ucp1^{Cre/+}$;$Atg12^{flox/flox}$ mice ($Atg12^{Ucp1}$ knockout [KO]) and $Ucp1^{Cre/+}$;$Atg5^{flox/flox}$ mice ($Atg5^{Ucp1}$ KO) (Figure S6A). $Atg5^{Ucp1}$ KO, $Atg12^{Ucp1}$ KO mice, or control mice ($Atg5^{flox/flox}$ or $Atg12^{flox/flox}$, respectively) were treated with the β3-AR agonist CL316,243 for 7 consecutive days (day 0 of β3-AR agonist withdrawal) and subsequently rested for 15 days after withdrawing β3-AR agonist (day 15 of withdrawal) (Figure 6A). We further confirmed that *Atg12* and *Atg5* were significantly reduced in beige adipocytes from $Atg12^{Ucp1}$ KO and $Atg5^{Ucp1}$ KO mice, respectively (Figure S6B).

As shown in Figure 6B, beige adipocyte biogenesis was highly induced both in control and $Atg12^{Ucp1}$ KO mice at day 0, as assessed by protein expression of UCP1, COX IV, and mitochondrial respiratory chain complexes. mtDNA transcripts and mRNA expression of nuclear-coded beige-enriched genes were significantly increased by chronic β3-AR agonist treatment both in control and $Atg12^{Ucp1}$ KO mice (Figure S6C). No difference was found in the basal expression levels of UCP1 and mitochondrial components in inguinal WAT between control and $Atg12^{Ucp1}$ KO mice without β3-AR agonist treatment. These results indicate that beige adipocyte differentiation per se is intact in $Atg12^{Ucp1}$ KO mice in response to chronic β3-AR agonist treatment. However, at 15 days post β3-AR agonist withdrawal, we observed a striking difference between control and $Atg12^{Ucp1}$ KO mice; the inguinal WAT from the $Atg12^{Ucp1}$ KO mice expressed higher levels of UCP1, COX IV, and mitochondrial respiratory chain complexes, as compared to that from control mice (Figure 6B). Importantly, a similar trend in UCP1 and mitochondrial protein expression was observed in the inguinal WAT from $Atg5^{Ucp1}$ KO mice (Figure 6C). Furthermore, mtDNA transcripts, such as *Nd2*, *Cox2*, and *Cox3*, were significantly higher in the inguinal WAT of $Atg12^{Ucp1}$ KO mice at day 15 following β3-AR agonist withdrawal (Figure 6D, left), whereas no significant differences in the mRNA expression of nuclear coded beige-enriched genes, such as *Pgc1a*, *Ucp1*, and *Cox7a*, were present between control and $Atg12^{Ucp1}$ KO mice (Figure 6D, right). The higher expression of UCP1 and mitochondrial proteins were preferentially found in beige adipocytes, with no major changes observed in classical brown adipocytes residing in interscapular BAT depots; rather, the interscapular BAT of $Atg12^{Ucp1}$ KO mice expressed similar levels of UCP1 and mitochondrial proteins as compared to control mice after β3-AR agonist withdrawal (Figure S6D). We also observed comparable, and in certain instances, lower levels of nuclear coded transcripts in the interscapular BAT of $Atg12^{Ucp1}$ KO mice as compared to that of control mice at day 0 and day 15 after β3-AR agonist withdrawal (not shown). Similarly, no major difference

(B) Kurtosis of the autophagy and lysosomal genes in (A). Note that the autophagy and lysosome component genes were platykurtic (K = −0.03 and −0.24, respectively), while randomly selected genes showed mesokurtic distribution (K = 1.07).

(C) Electron microscopy images of beige adipocytes during the transition (days 5–30 following β3-AR agonist withdrawal). Black arrowheads indicate the autophagic vesicles containing mitochondrial remnants, as identified by remaining cristae (red arrowheads). Scale bar, 500 nm.

(D) Confocal microscopy images of beige adipocytes from *GFP-LC3* mice. *GFP-LC3* mice were treated with saline or the β3-AR agonist CL316,243 for 7 consecutive days. The inguinal WAT depots were harvested at indicated time points (days 0–15) following β3-AR agonist withdrawal. Mitochondria and GFP-LC3-labeled autophagosomes were visualized by immunohistochemistry for Tom20 (red) and GFP (green), respectively. Nuclei are labeled with Hoechst (gray). The image in inset shows co-localization of GFP-LC3 and mitochondria. Scale bar, 12 μm.

(E) Quantification of the GFP-LC3 puncta in (A) at indicated time points. ***$p < 0.001$ by Mann-Whitney U test. n = 20–30 cells per condition.

(F) Autophagic flux in adipocytes from *GFP-LC3* mice at indicated time points (days 0–30) following β3-AR agonist withdrawal (beige adipocytes) and from *GFP-LC3* mice treated with saline (white adipocytes). x axis represents GFP-LC3 fluorescence intensity, and y axis represents the number of adipocytes normalized to mode. Data are representatives of two independent experiments.

(G) Immunoblotting for NBR1, p62/SQSTM1, and LC3 (LC3-I and LC3-II) from lysates of adipocytes isolated from the inguinal WAT of wild-type mice treated with saline or the β3-AR agonist CL316,243 (day 0 and 30 following β3-AR agonist withdrawal). β-actin was used as a loading control. Data are representatives of three independent experiments. Molecular weight (MW) is shown on the right.

See also Figure S4.

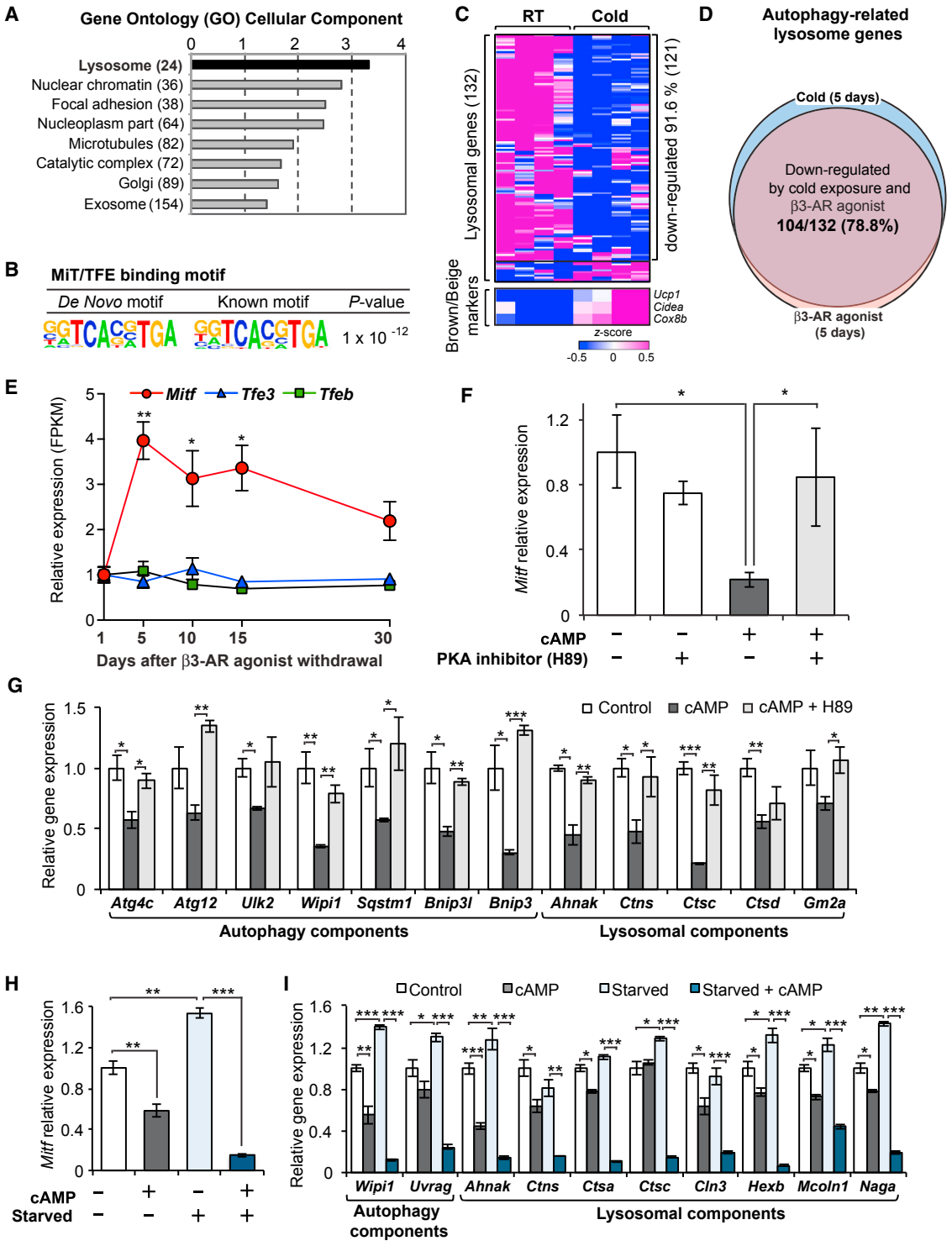

Figure 5. Regulation of Autophagy-Related Lysosome Biogenesis through the MiT/TFE Transcription Factors during the Beige-to-White Adipocyte Transition

(A) GO analysis (cellular component) of the genes that were transiently activated during the beige-to-white adipocyte transition (cluster 2).

(B) The HOMER-based motif analysis of lysosome genes in (A).

(C) Expression of lysosome marker genes in the inguinal WAT of mice housed under cold or ambient temperature for 5 days. FPKM values were converted to *Z* score and visualized in blue (low)-white (no change)-red (high) color scheme. n = 5.

(D) Regulation of the autophagy-related lysosome genes by cold exposure (shown in C) and by chronic β3-AR agonist treatment for 5 days. Note that 78.8% of the autophagy-related lysosome genes (104 out of 132 genes) were downregulated both by cold exposure and β3-AR agonist.

(legend continued on next page)

was observed in the expression of UCP1 and mitochondrial contents in the interscapular BAT depots between control and *Atg5*^{Ucp1} KO mice at day 0 and day 15 after β3-AR agonist withdrawal (Figure S6E).

Next, we asked whether *Ucp1*-specific deletion of *Atg12* similarly lead to high levels of mitochondria in the inguinal WAT after re-warming period following cold exposure. Consistent with the findings after β3-AR agonist withdrawal, we found that the inguinal WAT from the *Atg12*^{Ucp1} KO mice expressed higher levels of UCP1 and mitochondrial respiratory chain complexes, as compared to that from control mice at 15 days after re-warming (Figure S6F). We further asked whether pharmacological inhibition of autophagy was able to retain high levels of UCP1 and mitochondrial contents. To this end, we treated mice with chloroquine (CQ) at a dose of 60 mg kg^{-1} or saline for 15 consecutive days during the re-warming period following cold exposure (Figure 6E, top). We found that pharmacological inhibition of autophagy led to a significant retention of higher UCP1 levels and mitochondrial proteins in the inguinal WAT after re-warming (Figure 6E, bottom). Moreover, chloroquine treatment following β3-AR agonist withdrawal significantly induced LC3 accumulation in beige adipocytes (Figure S6G) and maintained higher levels of UCP1 and mitochondrial proteins in the inguinal WAT after β3-AR agonist withdrawal (Figure S6H). These data indicate that autophagy-mediated mitochondrial clearance via *Atg5* and *Atg12* is required for efficient beige-to-white adipocyte transition.

The distinct effects of autophagy deletion on beige adipocyte maintenance motivated the intriguing hypothesis that *Atg12*^{Ucp1} KO mice would exhibit higher thermogenic capacity after the removal of external cues. To test this hypothesis, we first measured oxygen consumption rate (OCR) of the inguinal WAT from control and *Atg12*^{Ucp1} KO mice at 15 days post β3-AR agonist withdrawal. As shown in Figure 6F, OCR was significantly higher in the inguinal WAT of *Atg12*^{Ucp1} KO mice than control mice when the tissues were treated with isoproterenol. In contrast, no significant difference was observed without isoproterenol treatment (at basal state). Thus, the beige adipocytes that persisted in *Atg12*^{Ucp1} KO were thermogenically active in response to cAMP stimulation.

To examine the metabolic significance of retaining thermogenic beige adipocytes in vivo, we next measured whole-body energy expenditure (VO_2) of control and *Atg12*^{Ucp1} KO mice during 17–18 days post β3-AR agonist withdrawal. As shown in Figure 6G, *Atg12*^{Ucp1} KO mice exhibited significantly higher VO_2 levels compared to control mice during the night phase. On the other hand, no significant difference was found in locomotor activity and food intake between control and *Atg12*^{Ucp1} KO mice (Figure S7A).

Prolonged Maintenance of Beige Adipocytes Prevents Diet-Induced Obesity and Insulin Resistance

Obesity is known to impair beige adipocyte biogenesis, partly through activation of transforming growth factor β (TGF-β) and Notch signals in WAT (Bi et al., 2014; Yadav et al., 2011). Here, we determine the extent to which obesity also affects the kinetics of beige-to-white adipocyte transition. To this end, we examined the morphological change of beige adipocytes in the inguinal WAT using *Ucp1-Cre;mT/mG* reporter mice under a regular diet (body weight, 29.5 ± 1.4 g) and age-matched obese mice under a high-fat diet for 12 weeks (body weight, 49.8 ± 0.8 g). We found that beige adipocytes (i.e., UCP1^{+}/GFP^{+} multilocular adipocytes) in the inguinal WAT of obese mice acquired a "white-like" state (i.e., unilocular lipids and loss of UCP1 expression) at a faster rate than age-matched lean mice (Figures 7A and 7B). On the other hand, no major change was found in the morphology of UCP1^{+} brown adipocytes between obese and lean mice (Figures S7B and S7C). This observation is intriguing because recent studies indicate that autophagy is altered in the adipose tissues of obese and type 2 diabetes patients (Jansen et al., 2012; Kosacka et al., 2015; Kovsan et al., 2011; Nunez et al., 2013; Ost et al., 2010). For instance, obesity-induced insulin resistance and type 2 diabetes impair mTOR signaling, thereby leading to autophagy activation in human adipose tissues (Kosacka et al., 2015; Ost et al., 2010). These results indicate that obesity not only impairs beige adipocyte differentiation but also accelerates the beige-to-white adipocyte transition, at least in part, through the activation of autophagy-lysosome biogenesis.

The above results motivated us to ask whether the persistence of thermogenic beige adipocytes in *Atg12*^{Ucp1} KO mice impacts weight gain in response to an obesogenic diet. Based on the previous observation that *Ucp1* deletion induces obesity specifically under conditions of thermoneutrality (Feldmann et al., 2009), individually-housed control and *Atg12*^{Ucp1} KO mice were chronically treated with the β3-AR agonist CL316,243 for 7 consecutive days to induce beige adipocyte development, and the mice were subsequently fed a high-fat diet for 8 weeks under thermoneutrality (Figure 7C). While there was no significant difference in body weight between control and *Atg12*^{Ucp1} KO mice immediately after β3-AR agonist treatment (day 0), *Atg12*^{Ucp1} KO mice gained significantly less body weight than

(E) Relative expression of MiT/TFE members of transcription factors (*Mitf*, *Tfe3*, and *Tfeb*) during the beige-to-white adipocyte transition. *p < 0.05, **p < 0.01 by two-tailed Student's t test. n = 3. Data are expressed as means ± SEM as compared to day 1 after β3-AR agonist treatment.

(F) Regulation of *Mitf* mRNA expression in response to cAMP in the presence or absence of a PKA inhibitor H89. Differentiated beige adipocytes were treated with 10 μM forskolin (cAMP) for 4 hr in the presence or absence of H89 at a dose of 10 μM. H89 was added 1 hr prior to forskolin treatment. *p < 0.05, by two-tailed Student's t test. n = 3. Data are expressed as means ± SEM.

(G) mRNA expression of autophagy components that are known targets of MiT/TFE transcription factors. *p < 0.05, **p < 0.01, ***p < 0.001 by two-tailed Student's t test. n = 3. Data are expressed as means ± SEM.

(H) Regulation of *Mitf* mRNA expression in response to cAMP in a regular medium or amino acid depletion medium (starved). Differentiated beige adipocytes were cultured in amino acid-free medium supplemented with 10% dialyzed serum for 4 hr prior to forskolin (cAMP) treatment (10 μM, 4 hr). **p < 0.01, ***p < 0.001 by two-tailed Student's t test. n = 3. Data are expressed as means ± SEM.

(I) mRNA expression of the MiT/TFE-target autophagy-related genes in response to cAMP under a fed or fasted state. *p < 0.05, **p < 0.01, ***p < 0.001 by two-tailed Student's t test. n = 3. Data are expressed as means ± SEM.

See also Figure S5 and Table S2.

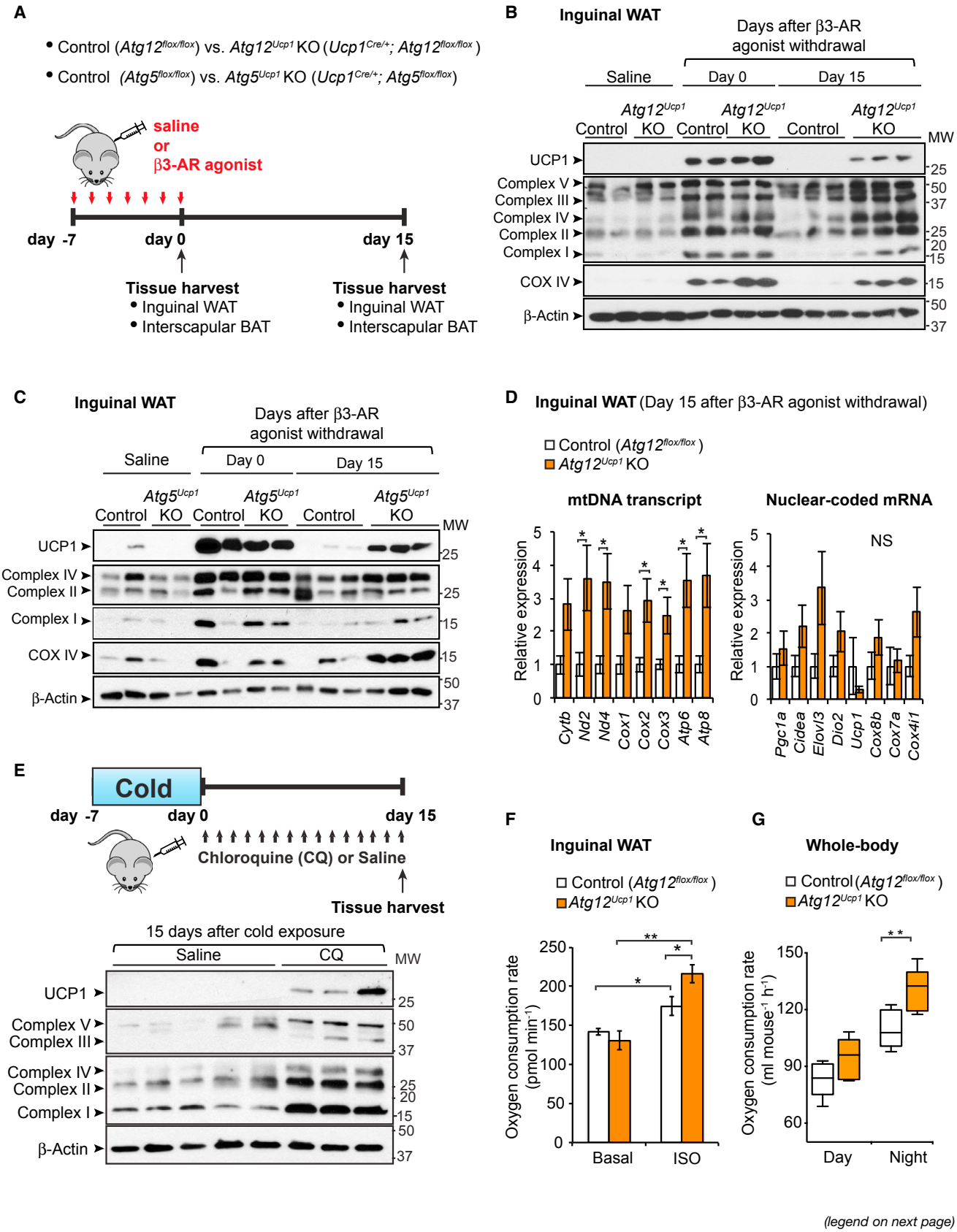

(legend on next page)

control mice after acclimation to thermoneutrality (Figure 7D). The difference in body weight between control and *Atg12*^{Ucp1} KO was due to a significantly reduced adipose mass, but not due to changes in lean mass (Figure 7E). Consistent with this result, white adipose tissue mass (inguinal WAT and epididymal WAT) in *Atg12*^{Ucp1} KO mice was lower than control mice (Figure 7F). Liver mass was slightly but significantly lower in *Atg12*^{Ucp1} KO mice, likely due to reduced hepatic triglyceride (TG) contents in *Atg12*^{Ucp1} KO mice (Figure 7G). Importantly, after 8 weeks of high-fat diet feeding, *Atg12*^{Ucp1} KO mice exhibited significantly improved systemic glucose homeostasis compared to control mice, as assessed by glucose-tolerance test (Figure 7H) and insulin-tolerance test (Figure 7I). In contrast, such metabolic phenotypes were not observed in the absence of β3-AR agonist treatment (Figures S7D–S7F). Thus, the metabolic phenotypes, i.e., reduced body-weight gain and improved glucose homeostasis, found in *Atg12*^{Ucp1} KO mice after β3-AR agonist treatment, are largely due to retention of thermogenically active beige adipocytes that are recruited by chronic β3-AR agonist treatment. These observations are consistent with the above finding that *Atg12*^{Ucp1} KO mice maintain higher amounts of UCP1 and other mitochondrial proteins in the inguinal WAT for prolonged periods compared to autophagy-competent controls, specifically following withdrawal of β3-AR agonist. Altogether, these data indicate that prolonged maintenance of thermogenically active beige fat is sufficient to increase whole-body energy expenditure and protect mice from diet-induced obesity and insulin resistance.

DISCUSSION

The present study demonstrates that autophagy-induced mitochondrial turnover is crucial for beige adipocyte maintenance and energy expenditure in vivo. Accumulating evidence shows that beige adipocyte biogenesis is induced by a variety of external stimuli, such as chronic cold exposure, exercise, long-term treatment of PPARγ agonists, cancer cachexia, and environmental enrichment (reviewed in Kajimura et al., 2015). The induced beige adipocytes appear to arise from de novo differentiation of beige precursors (Wang et al., 2013) or direct conversion from mature white adipocytes (Barbatelli et al., 2010; Himms-Hagen et al., 2000; Lee et al., 2015). Regardless of cellular origin, the newly recruited beige adipocytes gradually lose their morphological and molecular characteristics upon removal of external cues. Given the nature of lineage-tracing experiments, however, the prior studies were not able to determine whether this transition is mediated through de-differentiation of beige adipocytes to an intermediate precursor state and subsequent re-differentiation into white adipocytes, or through a direct conversion. Moreover, the inducible *Cre-ER* system used for the previous work may have certain technical limitations for lineage tracing; a recent study showed that newly recruited beige adipocytes during the chase phase (i.e., after tamoxifen withdrawal) may be unintentionally labeled because the hydrophobic properties of tamoxifen make it difficult to "wash-out" in adipose tissues (Ye et al., 2015). Our data provide direct evidence that beige adipocytes possess cell-intrinsic capacity to acquire a white-like state bypassing an intermediate precursor stage. Future analysis of chromatin reorganization and epigenetic regulation during this transition will additionally uncover the fundamental mechanisms by which environmental cues control beige adipocyte maintenance.

While recent studies reported a variety of external and internal cues that promote beige adipocyte differentiation, the molecular mechanism of beige adipocyte "maintenance" remains unknown. Genetic knockout of ATG7, the E1-like enzyme required for autophagosome formation, results in increased beige adipocytes in WAT, indicating a role of autophagy in beige adipocyte differentiation (Singh et al., 2009; Zhang et al., 2009). However these studies used *Fabp4-Cre* system, leading to knockout of ATG7 in all types of adipocytes and non-adipose tissues such as skeletal muscle and brain (Mullican et al., 2013). Thus, it remained unclear whether autophagy was involved in the specific differentiation of beige adipocyte from precursors, or maintenance of mature beige adipocytes. In addition, because ATG7 controls p53-dependent transcription and cell-cycle progression independently of its E1-like enzymatic activity, it is difficult to ascertain a general role for autophagy in those previous studies

Figure 6. Genetic Ablation of *Atg12* or *Atg5* Maintains Beige Adipocyte Characteristics after Removal of β3-AR Agonist

(A) Schematic illustration of experiments. Control (*Atg12*$^{flox/flox}$ or *Atg5*$^{flox/flox}$), *Atg12*^{Ucp1} KO (*Ucp1*$^{Cre/+}$;*Atg12*$^{flox/flox}$), and *Atg5*^{Ucp1} KO (*Ucp1*$^{Cre/+}$;*Atg5*$^{flox/flox}$) mice were treated with the β3-AR agonist CL316,243 for 7 consecutive days. Interscapular BAT and inguinal WAT depots were harvested for molecular analyses at day 0 and 15 following β3-AR agonist withdrawal.

(B) Immunoblotting for UCP1 and mitochondrial complexes (as indicated) in the inguinal WAT depots of control (*Atg12*$^{flox/flox}$) and *Atg12*^{Ucp1} KO mice at day 0 and day 15 following β3-AR agonist withdrawal. Inguinal WAT depots from control and *Atg12*^{Ucp1} KO mice treated with saline were included as a reference of basal expression of UCP1 and mitochondrial complexes. β-actin was used as a loading control. Molecular weight (MW) is shown on the right.

(C) Immunoblotting for UCP1 and mitochondrial complexes (as indicated) in the inguinal WAT depots of control (*Atg5*$^{flox/flox}$) and *Atg5*^{Ucp1} KO mice. Samples were harvested as illustrated in (B)

(D) Left: mitochondrial DNA (mtDNA) transcripts (as indicated) were quantified in the inguinal WAT depots of control and *Atg12*^{Ucp1} KO mice at day 15 following β3-AR agonist withdrawal. Right: mRNA levels of nuclear-coded beige-enriched markers (as indicated) are shown. *$p < 0.05$ by two-tailed Student's t test. $n = 5$. Data are expressed as means ± SEM.

(E) Top: wild-type mice were housed at 6°C for 7 days and subsequently kept under thermoneutrality (30°C) for 15 days. During the re-warming period, the mice were treated with chloroquine at a dose of 60 mg kg^{-1} or saline. Inguinal WAT depots were harvested for molecular analysis. Bottom: immunoblotting for UCP1 and mitochondrial complexes (as indicated) in the inguinal WAT of mice. Molecular weight (MW) is shown on the right.

(F) Oxygen consumption rate (OCR) in the inguinal WAT depots of control and *Atg12*^{Ucp1} KO mice at day 15 following β3-AR agonist withdrawal. The isolated tissues were treated with isoproterenol or vehicle (basal). OCR data were shown per 1 mg of tissue. *$p < 0.05$, **$p < 0.01$ by two-tailed Student's t test. $n = 4$. Data are expressed as means ± SEM.

(G) Quantification of whole-body oxygen consumption rate (VO_2) of control and *Atg12*^{Ucp1} KO mice during days 17–18 following β3-AR agonist withdrawal. VO_2 was measured by CLAMS during day and night time. **$p < 0.01$ by two-tailed Student's t test. $n = 5$ per genotype. Data are expressed as means ± SEM.

See also Figure S6.

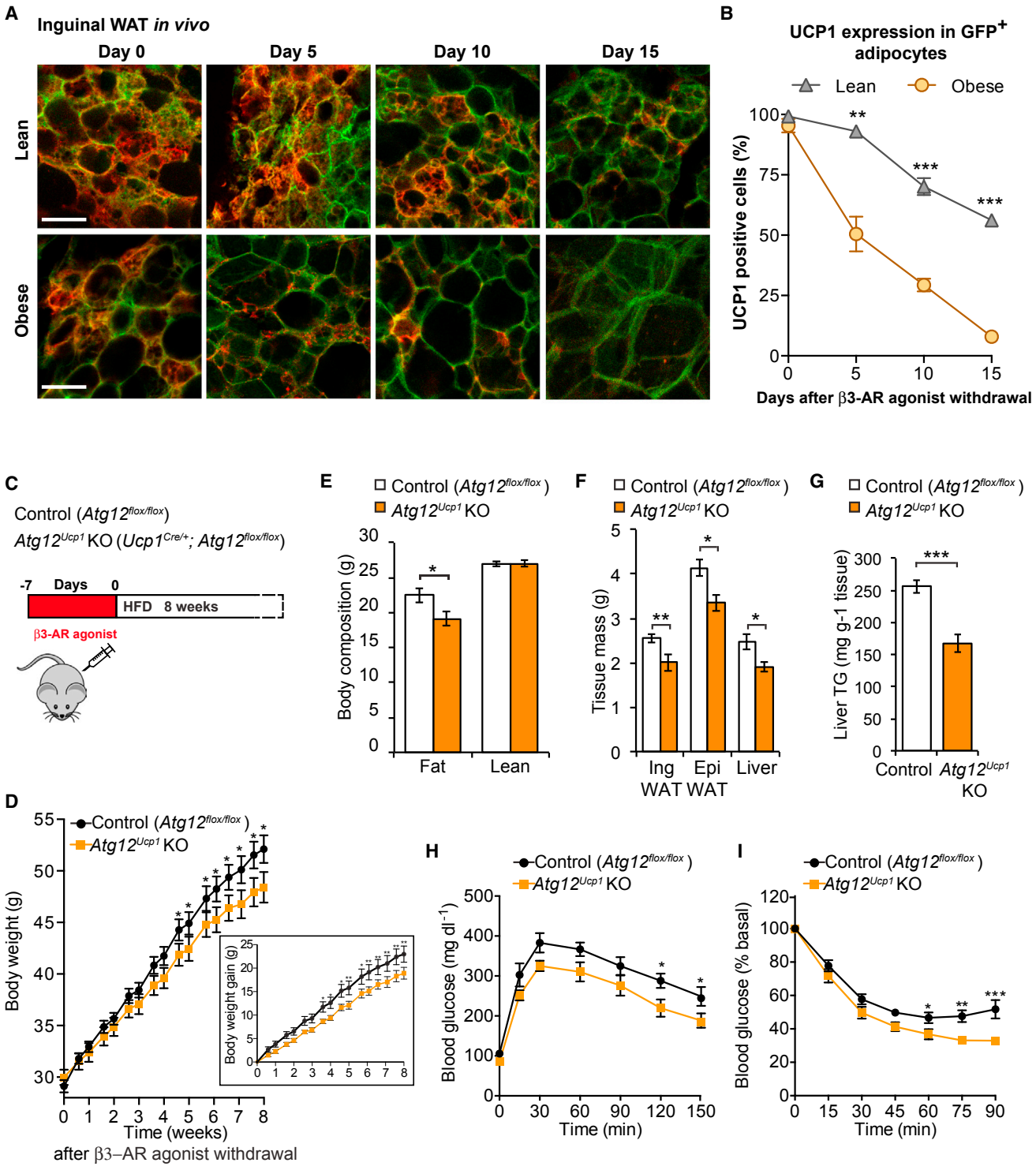

Figure 7. Prolonged Maintenance of Beige Adipocytes by Autophagy Inhibition Protects Animals from Diet-Induced Obesity and Insulin Resistance

(A) Confocal images of fixed inguinal WAT sections from *Ucp1*$^{Cre/+}$;*mT/mG* reporter mice. Inguinal WAT depots from lean mice under a regular diet (top) and age-matched obese mice under a high-fat diet (bottom) were immunostained for endogenous UCP1 (red). Note that the cellular membranes of beige adipocytes were visualized by membrane-targeted GFP (mGFP, green) of the mT/mG reporter mice. Scale bar, 57 μm.

(B) Quantification of mGFP-positive adipocytes in lean and obese mice that express endogenous UCP1 in (A). n = 100 cells or more per group. **p < 0.01, ***p < 0.001 by two-tailed Student's t test. Data are expressed as means ± SEM.

(legend continued on next page)

(Lee et al., 2012a). Thus, we selectively deleted either *Atg5* or *Atg12* in differentiated beige/brown adipocytes using *Ucp1-Cre* in order to test the specific requirement of autophagy for beige adipocyte maintenance per se. While ATG5 and ATG12 each possess unique functions in other cell types (Kimmey et al., 2015; Malhotra et al., 2015), we demonstrate that genetic deletion of *Atg5* or *Atg12* in beige adipocytes exhibit highly concordant phenotypes, most notably, the substantial retention of UCP1 and mitochondrial proteins in the subcutaneous WAT after withdrawing β3-AR agonist (Figure 6). These results strongly argue against any individual effects exerted by these ATGs. In further support, pharmacological autophagy inhibition with the antimalarial chloroquine retains high levels of UCP1 and mitochondrial proteins after re-warming following cold exposure as well as after β3-AR agonist withdrawal. Taken together, these results, obtained using genetic and pharmacological approaches, corroborate a critical requirement for the autophagy pathway in clearance of beige adipocyte mitochondria during the beige-to-white transition in vivo, thereby intimating a specific role of mitophagy in beige adipocyte maintenance.

Recent studies reported that adult human BAT from supraclavicular regions displays molecular signatures that resemble beige adipocytes (Lidell et al., 2013; Sharp et al., 2012; Shinoda et al., 2015a; Wu et al., 2012) and that chronic cold acclimation increases glucose uptake in the BAT of adult humans who do not possess detectable BAT before cold treatment (Lee et al., 2014b; van der Lans et al., 2013; Yoneshiro et al., 2013). These studies indicate that adult humans possess beige-like "recruitable" thermogenic adipocytes. Notably, the prevalence of human BAT is inversely correlated with BMI and adiposity (Cypess et al., 2009; Saito et al., 2009; van Marken Lichtenbelt et al., 2009), whereas autophagy is upregulated in adipose tissue of obese subjects, exhibiting a positive correlation with the degree of obesity and visceral fat distribution (Jansen et al., 2012; Kosacka et al., 2015; Kovsan et al., 2011; Nunez et al., 2013; Ost et al., 2010). Our studies in rodents also indicate that obesity accelerates the beige-to-white adipocyte transition. It is conceivable that the altered kinetics of the transition under obesity is due partly to the activation of autophagy-related lysosome biogenesis; thus, autophagy/lysosome inhibition can be an effective approach to retain high thermogenically active beige adipocytes for prolonged period.

It has been appreciated that classical brown adipocytes in the interscapular BAT can acquire a "white-like" unilocular morphology in morbidly obese mice, such as *ob/ob* mice, or in aged mice (Cinti, 1999; Sellayah and Sikder, 2014). Our experiments, on the other hand, were performed in young mice under a relatively short-term high fat diet (4–8 weeks) in which mitochondrial biogenesis remained active in the BAT. It is likely that mitochondrial biogenesis rather than mitochondrial clearance largely contributes to the maintenance of high mitochondrial contents in BAT, whereas mitochondrial clearance plays a critical role in the mitochondrial homeostasis of beige fat particularly when external cues are withdrawn. Our data, however, do not exclude the possibility that autophagy-mediated mitochondrial clearance also play a role in the maintenance of classical brown adipocytes in morbidly obese mice or aged mice.

In summary, the present study identified autophagy-mediated mitochondrial clearance as a previously unappreciated mechanism that controls beige adipocyte maintenance and whole-body energy homeostasis. This may offer a new therapeutic opportunity to combat obesity and insulin resistance through prolonged maintenance of thermogenic beige adipocytes.

EXPERIMENTAL PROCEDURES

Animals

All animal experiments were performed under the guidelines established by the UCSF Institutional Animal Care and Use Committee. Details of the transgene design can be found in the Supplemental Experimental Procedures. To visualize brown and beige adipocytes in vivo, $Ucp1^{Cre/+}$ mice were crossed with Rosa26-GFP or mT/mG mice (The Jackson Laboratory). To induce beige adipocyte biogenesis, the β3-AR agonist CL316,243 (Sigma) was administered intraperitoneally to male mice at a dose of 1 mg kg^{-1} for 7 consecutive days. To assess the basal amount of GFP-positive cells present in adipose tissues prior to β3-AR agonist treatment, mice were bred and treated with β3-AR agonist at thermoneutrality (30°C). For cold exposure experiments, animals were single-caged and exposed to 6°C for 5–7 days.

Ex Vivo Monitoring of Beige and Brown Adipocytes

Mature adipocytes from the inguinal WAT and interscapular BAT depots of CL316,243-treated *Ucp1*$^{Cre/+}$*;Rosa26-GFP* mice were isolated by fractionation, embedded in collagen gel containing 2.5 mg ml^{-1} Collagen I (BD354236), 1 μg ml^{-1} Fibronectin (Millipore), and 0.1% BSA. The cell-containing gel was allowed to solidify at 37°C for 30 min and cultured in DMEM supplemented with 10% FBS. Culture medium did not contain any stimuli, such as β3-AR agonist, that control beige adipocyte differentiation. Individual

(C) Schematic of the metabolic experiment in control (*Atg12*$^{flox/flox}$) and *Atg12*^{Ucp1} KO mice. Control and *Atg12*^{Ucp1} KO mice were treated with CL316,243 for 7 days to induce beige adipocyte biogenesis. Subsequently, the mice were acclimated to thermoneutrality (30°C) under a high-fat diet for 8 weeks.
(D) Body weight of control (*Atg12*$^{flox/flox}$) and *Atg12*^{Ucp1} KO mice under a high-fat diet. Body weight was measured twice a week. *$p < 0.05$, **$p < 0.01$. n = 8–10 per genotype. The graph in the inset shows body weight gain of control and *Atg12*^{Ucp1} KO mice. Significance was determined by two-way repeated-measures ANOVA followed by Fisher's LSD test. Data are expressed as means ± SEM.
(E) Body composition of control (*Atg12*$^{flox/flox}$) and *Atg12*^{Ucp1} KO mice from (D) at the end of 8 weeks of high-fat diet. *$p < 0.05$ by two-tailed Student's t test. Data are expressed as means ± SEM.
(F) Tissue weight of inguinal WAT, epididymal WAT, and liver from control (*Atg12*$^{flox/flox}$) and *Atg12*^{Ucp1} KO mice from (D) after 9 weeks of high fat diet. *$p < 0.05$, **$p < 0.01$. Data are expressed as means ± SEM.
(G) Liver triglyceride levels in control (*Atg12*$^{flox/flox}$) and *Atg12*^{Ucp1} KO mice after 9 weeks of high fat diet. ***$p < 0.001$. Data are expressed as means ± SEM.
(H) After 8 weeks of high-fat diet, control (*Atg12*$^{flox/flox}$) and *Atg12*^{Ucp1} KO mice were fasted for 12 hr and injected with 1.5g kg^{-1} glucose. Whole-body glucose was measured at 15, 30, 60, 90, 120, and 150 min. *$p < 0.05$, n = 6–8 per genotype. Significance was determined by two-way repeated-measures ANOVA followed by Fisher's LSD test. Data are expressed as means ± SEM.
(I) After 8.5 weeks of high fat diet, control (*Atg12*$^{flox/flox}$) and *Atg12*^{Ucp1} KO mice were fasted for 3 hr and injected with 0.75 U kg^{-1} insulin. Whole-body glucose was measured at 15, 30, 45, 60, 75, and 90 min. *$p < 0.05$, **$p < 0.01$, ***$p < 0.001$, n = 7–8 per genotype. Significance was determined by two-way repeated-measures ANOVA followed by Fisher's LSD test. Data are expressed as means ± SEM.
See also Figure S7.

live GFP$^+$ adipocytes were traced daily for 10 consecutive days using the In Cell Analyzer 2000 to define and re-image the position of interest over time. Images were processed using In Cell Developer Toolbox V1.8 (GE Healthcare Life Sciences) and Volocity 6.1.1 software (Improvision).

Flow Cytometry

To isolate GFP-positive adipocytes, inguinal WAT depots from *Ucp1*$^{Cre/+}$*;Rosa26-GFP* or Adiponectin$^{Cre/+}$*;Rosa26-GFP* mice were digested to single cells according to the previous study (Ohno et al., 2012). Adipocytes were first gated based on size and granularity. Live GFP-positive cells were gated based on GFP-negative control cells from wild-type mice not expressing GFP.

RNA Sequencing and Bioinformatics

Total RNA was extracted from FACS-isolated GFP-positive adipocytes or preadipocytes using the RNeasy Micro Kit (QIAGEN). Libraries were constructed from minimum of 22 ng of total RNA as previously described (Shinoda et al., 2015a). High-throughput sequencing was performed using a HiSeq 2500 instrument (Illumina) at the UCSF Institute for Human Genetics core facility. Reproducibility of the RNA sequencing data was confirmed by sequencing the identical RNA samples (R^2 = 0.983). The data were deposited in ArrayExpress (http://www.ebi.ac.uk/arrayexpress/) under accession number ArrayExpress: E-MTAB-3978.

Clustering of genes was performed as follows: the fragments per kilobase million (FPKM) profiles of genes at several time points (days 0–30 of β3-AR agonist withdrawal) were *Z* transformed, as such, the mean for each gene was zero and SD was one. The Fuzzy C-Means (FCM) clustering analysis was described elsewhere (Olsen et al., 2006). The top 10,000 highly expressed genes were used for the clustering. The FCM parameters were c = 9 and m = 1.15, respectively. For principal component analysis (PCA), preadipocytes and white adipocytes were first mapped onto two-dimensional (PC1 and PC2) space, based on the expression of 10,138 genes that showed differences between the two groups by 2-fold or more. The transcriptome of GFP-positive adipocytes at each time point (days 0–30) was mapped on the same PC plot, based on the expression levels of 10,138 genes. Similar PC plots were reproducibly found when a different number of genes (2,000, 1,000, or 500) was applied.

Metabolic Studies

Ten-week-old *Atg12*^{Ucp1} KO mice (*Ucp1*$^{Cre/+}$*;Atg12*$^{flox/flox}$) and littermate control mice (*Atg12*$^{flox/flox}$) were treated with β3-AR agonist for 7 days and maintained at thermoneutrality during β3-AR agonist withdrawal. Whole-body energy expenditure was measured between 17 and 18 days after β3-AR agonist withdrawal using a Comprehensive Lab Animal Monitoring System (CLAMS, Columbus Instruments). Locomotor activity was simultaneously monitored by the CLAMS. For diet-induced obesity study, 9-week-old *Atg12*^{Ucp1} KO and control (*Atg12*$^{flox/flox}$) male mice were fed a high-fat diet. Following 7-day β3-AR agonist treatment, mice were transferred to thermoneutrality (30°C) for 8 weeks. Body weight was measured twice per week. Glucose tolerance test experiments were performed at 8 weeks or 12 weeks of high-fat diet. Insulin tolerance test was performed after 8.5 weeks of high-fat diet.

ACCESSION NUMBERS

The accession number for the RNA sequencing reported in this paper is ArrayExpress: E-MTAB-3978.

SUPPLEMENTAL INFORMATION

Supplemental Information includes Supplemental Experimental Procedures, seven figures, and two tables and can be found with this article online at http://dx.doi.org/10.1016/j.cmet.2016.08.002.

AUTHOR CONTRIBUTIONS

S.A.-K. and S.K. conceived the study, designed experiments, and analyzed and interpreted the data. K.S. performed bioinformatics analyses. S.A.-K., Y.H., K.I., H.H., and Q.K. performed experiments and interpreted the data. Y.Y. provided technical help. R.P. and J.D. provided reagents and expertise in the field of autophagy. S.A.-K. and S.K. wrote the manuscript. S.A.-K., R.P., J.D., and S.K. edited the manuscript.

ACKNOWLEDGMENTS

We are grateful to Dr. Luke Cassereau and Dr. Valerie Weaver at University of California, San Francisco for their help in developing the single-cell monitoring system, Anthony Jose from the FACS Core for his help in isolating mature adipocytes, Dr. Noboru Mizushima at the University of Tokyo for providing *GFP-LC3* mice, Dr. Evan Rosen at Beth Israel Deaconess Medical Center and Harvard Medical School for providing *Ucp1*$^{Cre/+}$ mice, Dr. Christophe Paillart for his help in the CLAMS studies, and Larry Ackerman for his help with EM. We acknowledge support from the NIH (DK97441 and DK108822), the Diabetes and Endocrine-Related Disease Center (DERC) (DK63720), the Pew Charitable Trust, and the Japan Science and Technology Agency (to S.K.), NIH CA126792 (to J.D.), the American Cancer Society, and the Pancreatic Cancer Action Network-AACR Career Development award (to R.M.P.). S.A.-K. is supported by American Heart Association (AHA) grant 15PRE23050029 and the California Institute for Regenerative Medicine (CIRM) grant TG2-01153. K.S. is supported by the Larry L. Hillblom Foundation (LLHF) grant 2014-D-025-FEL. Y.H. and K.I. are supported by the Manpei Suzuki Diabetes Foundation. Q.K. is supported by the China Scholarship Council (CSC) grant 201506350063.

Received: January 13, 2016
Revised: June 6, 2016
Accepted: July 29, 2016
Published: August 25, 2016

REFERENCES

Atit, R., Sgaier, S.K., Mohamed, O.A., Taketo, M.M., Dufort, D., Joyner, A.L., Niswander, L., and Conlon, R.A. (2006). Beta-catenin activation is necessary and sufficient to specify the dorsal dermal fate in the mouse. Dev. Biol. *296*, 164–176.

Barbatelli, G., Murano, I., Madsen, L., Hao, Q., Jimenez, M., Kristiansen, K., Giacobino, J.P., De Matteis, R., and Cinti, S. (2010). The emergence of cold-induced brown adipocytes in mouse white fat depots is determined predominantly by white to brown adipocyte transdifferentiation. Am. J. Physiol. Endocrinol. Metab. *298*, E1244–E1253.

Bi, P., Shan, T., Liu, W., Yue, F., Yang, X., Liang, X.R., Wang, J., Li, J., Carlesso, N., Liu, X., and Kuang, S. (2014). Inhibition of Notch signaling promotes browning of white adipose tissue and ameliorates obesity. Nat. Med. *20*, 911–918.

Bowman, C.J., Ayer, D.E., and Dynlacht, B.D. (2014). Foxk proteins repress the initiation of starvation-induced atrophy and autophagy programs. Nat. Cell Biol. *16*, 1202–1214.

Cederberg, A., Grønning, L.M., Ahrén, B., Taskén, K., Carlsson, P., and Enerbäck, S. (2001). FOXC2 is a winged helix gene that counteracts obesity, hypertriglyceridemia, and diet-induced insulin resistance. Cell *106*, 563–573.

Chauhan, S., Goodwin, J.G., Chauhan, S., Manyam, G., Wang, J., Kamat, A.M., and Boyd, D.D. (2013). ZKSCAN3 is a master transcriptional repressor of autophagy. Mol. Cell *50*, 16–28.

Cinti, S. (1999). The Adipose Organ (Milano, Italy: Editrice Kurtis).

Cypess, A.M., Lehman, S., Williams, G., Tal, I., Rodman, D., Goldfine, A.B., Kuo, F.C., Palmer, E.L., Tseng, Y.H., Doria, A., et al. (2009). Identification and importance of brown adipose tissue in adult humans. N. Engl. J. Med. *360*, 1509–1517.

Feldmann, H.M., Golozoubova, V., Cannon, B., and Nedergaard, J. (2009). UCP1 ablation induces obesity and abolishes diet-induced thermogenesis in mice exempt from thermal stress by living at thermoneutrality. Cell Metab. *9*, 203–209.

Gospodarska, E., Nowialis, P., and Kozak, L.P. (2015). Mitochondrial turnover: a phenotype distinguishing brown adipocytes from interscapular brown adipose tissue and white adipose tissue. J. Biol. Chem. *290*, 8243–8255.

Guerra, C., Koza, R.A., Yamashita, H., Walsh, K., and Kozak, L.P. (1998). Emergence of brown adipocytes in white fat in mice is under genetic control. Effects on body weight and adiposity. J. Clin. Invest. *102*, 412–420.

He, C., and Klionsky, D.J. (2009). Regulation mechanisms and signaling pathways of autophagy. Annu. Rev. Genet. *43*, 67–93.

Heinz, S., Benner, C., Spann, N., Bertolino, E., Lin, Y.C., Laslo, P., Cheng, J.X., Murre, C., Singh, H., and Glass, C.K. (2010). Simple combinations of lineage-determining transcription factors prime cis-regulatory elements required for macrophage and B cell identities. Mol. Cell *38*, 576–589.

Himms-Hagen, J., Melnyk, A., Zingaretti, M.C., Ceresi, E., Barbatelli, G., and Cinti, S. (2000). Multilocular fat cells in WAT of CL-316243-treated rats derive directly from white adipocytes. Am. J. Physiol. Cell Physiol. *279*, C670–C681.

Jansen, H.J., van Essen, P., Koenen, T., Joosten, L.A., Netea, M.G., Tack, C.J., and Stienstra, R. (2012). Autophagy activity is up-regulated in adipose tissue of obese individuals and modulates proinflammatory cytokine expression. Endocrinology *153*, 5866–5874.

Kajimura, S., Seale, P., Tomaru, T., Erdjument-Bromage, H., Cooper, M.P., Ruas, J.L., Chin, S., Tempst, P., Lazar, M.A., and Spiegelman, B.M. (2008). Regulation of the brown and white fat gene programs through a PRDM16/CtBP transcriptional complex. Genes Dev. *22*, 1397–1409.

Kajimura, S., Spiegelman, B.M., and Seale, P. (2015). Brown and beige fat: physiological roles beyond heat generation. Cell Metab. *22*, 546–559.

Kim, K.H., Jeong, Y.T., Oh, H., Kim, S.H., Cho, J.M., Kim, Y.N., Kim, S.S., Kim, H., Hur, K.Y., Kim, H.K., et al. (2013). Autophagy deficiency leads to protection from obesity and insulin resistance by inducing Fgf21 as a mitokine. Nat. Med. *19*, 83–92.

Kimmey, J.M., Huynh, J.P., Weiss, L.A., Park, S., Kambal, A., Debnath, J., Virgin, H.W., and Stallings, C.L. (2015). Unique role for ATG5 in neutrophil-mediated immunopathology during M. tuberculosis infection. Nature *528*, 565–569.

Klionsky, D.J., Abdelmohsen, K., Abe, A., Abedin, M.J., Abeliovich, H., Acevedo Arozena, A., Adachi, H., Adams, C.M., Adams, P.D., Adeli, K., et al. (2016). Guidelines for the use and interpretation of assays for monitoring autophagy (3rd edition). Autophagy *12*, 1–222.

Kong, X., Banks, A., Liu, T., Kazak, L., Rao, R.R., Cohen, P., Wang, X., Yu, S., Lo, J.C., Tseng, Y.H., et al. (2014). IRF4 is a key thermogenic transcriptional partner of PGC-1α. Cell *158*, 69–83.

Kosacka, J., Kern, M., Klöting, N., Paeschke, S., Rudich, A., Haim, Y., Gericke, M., Serke, H., Stumvoll, M., Bechmann, I., et al. (2015). Autophagy in adipose tissue of patients with obesity and type 2 diabetes. Mol. Cell. Endocrinol. *409*, 21–32.

Kovsan, J., Blüher, M., Tarnovscki, T., Klöting, N., Kirshtein, B., Madar, L., Shai, I., Golan, R., Harman-Boehm, I., Schön, M.R., et al. (2011). Altered autophagy in human adipose tissues in obesity. J. Clin. Endocrinol. Metab. *96*, E268–E277.

Lee, I.H., Kawai, Y., Fergusson, M.M., Rovira, I.I., Bishop, A.J., Motoyama, N., Cao, L., and Finkel, T. (2012a). Atg7 modulates p53 activity to regulate cell cycle and survival during metabolic stress. Science *336*, 225–228.

Lee, Y.H., Petkova, A.P., Mottillo, E.P., and Granneman, J.G. (2012b). In vivo identification of bipotential adipocyte progenitors recruited by β3-adrenoceptor activation and high-fat feeding. Cell Metab. *15*, 480–491.

Lee, J.M., Wagner, M., Xiao, R., Kim, K.H., Feng, D., Lazar, M.A., and Moore, D.D. (2014a). Nutrient-sensing nuclear receptors coordinate autophagy. Nature *516*, 112–115.

Lee, P., Smith, S., Linderman, J., Courville, A.B., Brychta, R.J., Dieckmann, W., Werner, C.D., Chen, K.Y., and Celi, F.S. (2014b). Temperature-acclimated brown adipose tissue modulates insulin sensitivity in humans. Diabetes *63*, 3686–3698.

Lee, Y.H., Petkova, A.P., Konkar, A.A., and Granneman, J.G. (2015). Cellular origins of cold-induced brown adipocytes in adult mice. FASEB J. *29*, 286–299.

Lidell, M.E., Betz, M.J., Dahlqvist Leinhard, O., Heglind, M., Elander, L., Slawik, M., Mussack, T., Nilsson, D., Romu, T., Nuutila, P., et al. (2013). Evidence for two types of brown adipose tissue in humans. Nat. Med. *19*, 631–634.

Liu, D., Bordicchia, M., Zhang, C., Fang, H., Wei, W., Li, J.L., Guilherme, A., Guntur, K., Czech, M.P., and Collins, S. (2016). Activation of mTORC1 is essential for β-adrenergic stimulation of adipose browning. J. Clin. Invest. *126*, 1704–1716.

Malhotra, R., Warne, J.P., Salas, E., Xu, A.W., and Debnath, J. (2015). Loss of Atg12, but not Atg5, in pro-opiomelanocortin neurons exacerbates diet-induced obesity. Autophagy *11*, 145–154.

Mizushima, N., and Komatsu, M. (2011). Autophagy: renovation of cells and tissues. Cell *147*, 728–741.

Mizushima, N., Yamamoto, A., Matsui, M., Yoshimori, T., and Ohsumi, Y. (2004). In vivo analysis of autophagy in response to nutrient starvation using transgenic mice expressing a fluorescent autophagosome marker. Mol. Biol. Cell *15*, 1101–1111.

Mullican, S.E., Tomaru, T., Gaddis, C.A., Peed, L.C., Sundaram, A., and Lazar, M.A. (2013). A novel adipose-specific gene deletion model demonstrates potential pitfalls of existing methods. Mol. Endocrinol. *27*, 127–134.

Nunez, C.E., Rodrigues, V.S., Gomes, F.S., Moura, R.F., Victorio, S.C., Bombassaro, B., Chaim, E.A., Pareja, J.C., Geloneze, B., Velloso, L.A., et al. (2013). Defective regulation of adipose tissue autophagy in obesity. Int. J. Obes. (Lond.) *37*, 1473–1480.

Ohno, H., Shinoda, K., Spiegelman, B.M., and Kajimura, S. (2012). PPARγ agonists induce a white-to-brown fat conversion through stabilization of PRDM16 protein. Cell Metab. *15*, 395–404.

Ohyama, K., Nogusa, Y., Shinoda, K., Suzuki, K., Bannai, M., and Kajimura, S. (2016). A synergistic antiobesity effect by a combination of capsinoids and cold temperature through promoting beige adipocyte biogenesis. Diabetes *65*, 1410–1423.

Olsen, J.V., Blagoev, B., Gnad, F., Macek, B., Kumar, C., Mortensen, P., and Mann, M. (2006). Global, in vivo, and site-specific phosphorylation dynamics in signaling networks. Cell *127*, 635–648.

Ost, A., Svensson, K., Ruishalme, I., Brännmark, C., Franck, N., Krook, H., Sandström, P., Kjolhede, P., and Strålfors, P. (2010). Attenuated mTOR signaling and enhanced autophagy in adipocytes from obese patients with type 2 diabetes. Mol. Med. *16*, 235–246.

Perera, R.M., Stoykova, S., Nicolay, B.N., Ross, K.N., Fitamant, J., Boukhali, M., Lengrand, J., Deshpande, V., Selig, M.K., Ferrone, C.R., et al. (2015). Transcriptional control of autophagy-lysosome function drives pancreatic cancer metabolism. Nature *524*, 361–365.

Rosenwald, M., Perdikari, A., Rülicke, T., and Wolfrum, C. (2013). Bi-directional interconversion of brite and white adipocytes. Nat. Cell Biol. *15*, 659–667.

Saito, M., Okamatsu-Ogura, Y., Matsushita, M., Watanabe, K., Yoneshiro, T., Nio-Kobayashi, J., Iwanaga, T., Miyagawa, M., Kameya, T., Nakada, K., et al. (2009). High incidence of metabolically active brown adipose tissue in healthy adult humans: effects of cold exposure and adiposity. Diabetes *58*, 1526–1531.

Sanchez-Gurmaches, J., Hung, C.M., Sparks, C.A., Tang, Y., Li, H., and Guertin, D.A. (2012). PTEN loss in the Myf5 lineage redistributes body fat and reveals subsets of white adipocytes that arise from Myf5 precursors. Cell Metab. *16*, 348–362.

Sardiello, M., Palmieri, M., di Ronza, A., Medina, D.L., Valenza, M., Gennarino, V.A., Di Malta, C., Donaudy, F., Embrione, V., Polishchuk, R.S., et al. (2009). A gene network regulating lysosomal biogenesis and function. Science *325*, 473–477.

Schulz, T.J., Huang, T.L., Tran, T.T., Zhang, H., Townsend, K.L., Shadrach, J.L., Cerletti, M., McDougall, L.E., Giorgadze, N., Tchkonia, T., et al. (2011). Identification of inducible brown adipocyte progenitors residing in skeletal muscle and white fat. Proc. Natl. Acad. Sci. USA *108*, 143–148.

Seale, P., Bjork, B., Yang, W., Kajimura, S., Chin, S., Kuang, S., Scimè, A., Devarakonda, S., Conroe, H.M., Erdjument-Bromage, H., et al. (2008). PRDM16 controls a brown fat/skeletal muscle switch. Nature *454*, 961–967.

Seale, P., Conroe, H.M., Estall, J., Kajimura, S., Frontini, A., Ishibashi, J., Cohen, P., Cinti, S., and Spiegelman, B.M. (2011). Prdm16 determines the

thermogenic program of subcutaneous white adipose tissue in mice. J. Clin. Invest. *121*, 96–105.

Sellayah, D., and Sikder, D. (2014). Orexin restores aging-related brown adipose tissue dysfunction in male mice. Endocrinology *155*, 485–501.

Seok, S., Fu, T., Choi, S.E., Li, Y., Zhu, R., Kumar, S., Sun, X., Yoon, G., Kang, Y., Zhong, W., et al. (2014). Transcriptional regulation of autophagy by an FXR-CREB axis. Nature *516*, 108–111.

Settembre, C., Di Malta, C., Polito, V.A., Garcia Arencibia, M., Vetrini, F., Erdin, S., Erdin, S.U., Huynh, T., Medina, D., Colella, P., et al. (2011). TFEB links autophagy to lysosomal biogenesis. Science *332*, 1429–1433.

Sharp, L.Z., Shinoda, K., Ohno, H., Scheel, D.W., Tomoda, E., Ruiz, L., Hu, H., Wang, L., Pavlova, Z., Gilsanz, V., and Kajimura, S. (2012). Human BAT possesses molecular signatures that resemble beige/brite cells. PLoS ONE *7*, e49452.

Shinoda, K., Luijten, I.H., Hasegawa, Y., Hong, H., Sonne, S.B., Kim, M., Xue, R., Chondronikola, M., Cypess, A.M., Tseng, Y.H., et al. (2015a). Genetic and functional characterization of clonally derived adult human brown adipocytes. Nat. Med. *21*, 389–394.

Shinoda, K., Ohyama, K., Hasegawa, Y., Chang, H.Y., Ogura, M., Sato, A., Hong, H., Hosono, T., Sharp, L.Z., Scheel, D.W., et al. (2015b). Phosphoproteomics identifies CK2 as a negative regulator of beige adipocyte thermogenesis and energy expenditure. Cell Metab. *22*, 997–1008.

Shvets, E., Fass, E., and Elazar, Z. (2008). Utilizing flow cytometry to monitor autophagy in living mammalian cells. Autophagy *4*, 621–628.

Singh, R., Xiang, Y., Wang, Y., Baikati, K., Cuervo, A.M., Luu, Y.K., Tang, Y., Pessin, J.E., Schwartz, G.J., and Czaja, M.J. (2009). Autophagy regulates adipose mass and differentiation in mice. J. Clin. Invest. *119*, 3329–3339.

van der Lans, A.A., Hoeks, J., Brans, B., Vijgen, G.H., Visser, M.G., Vosselman, M.J., Hansen, J., Jörgensen, J.A., Wu, J., Mottaghy, F.M., et al. (2013). Cold acclimation recruits human brown fat and increases nonshivering thermogenesis. J. Clin. Invest. *123*, 3395–3403.

van Marken Lichtenbelt, W.D., Vanhommerig, J.W., Smulders, N.M., Drossaerts, J.M., Kemerink, G.J., Bouvy, N.D., Schrauwen, P., and Teule, G.J. (2009). Cold-activated brown adipose tissue in healthy men. N. Engl. J. Med. *360*, 1500–1508.

Wang, Q.A., Tao, C., Gupta, R.K., and Scherer, P.E. (2013). Tracking adipogenesis during white adipose tissue development, expansion and regeneration. Nat. Med. *19*, 1338–1344.

Wang, W., Kissig, M., Rajakumari, S., Huang, L., Lim, H.W., Won, K.J., and Seale, P. (2014). Ebf2 is a selective marker of brown and beige adipogenic precursor cells. Proc. Natl. Acad. Sci. USA *111*, 14466–14471.

Warr, M.R., Binnewies, M., Flach, J., Reynaud, D., Garg, T., Malhotra, R., Debnath, J., and Passegué, E. (2013). FOXO3A directs a protective autophagy program in haematopoietic stem cells. Nature *494*, 323–327.

Wu, J., Boström, P., Sparks, L.M., Ye, L., Choi, J.H., Giang, A.H., Khandekar, M., Virtanen, K.A., Nuutila, P., Schaart, G., et al. (2012). Beige adipocytes are a distinct type of thermogenic fat cell in mouse and human. Cell *150*, 366–376.

Xue, B., Rim, J.S., Hogan, J.C., Coulter, A.A., Koza, R.A., and Kozak, L.P. (2007). Genetic variability affects the development of brown adipocytes in white fat but not in interscapular brown fat. J. Lipid Res. *48*, 41–51.

Yadav, H., Quijano, C., Kamaraju, A.K., Gavrilova, O., Malek, R., Chen, W., Zerfas, P., Zhigang, D., Wright, E.C., Stuelten, C., et al. (2011). Protection from obesity and diabetes by blockade of TGF-β/Smad3 signaling. Cell Metab. *14*, 67–79.

Ye, R., Wang, Q.A., Tao, C., Vishvanath, L., Shao, M., McDonald, J.G., Gupta, R.K., and Scherer, P.E. (2015). Impact of tamoxifen on adipocyte lineage tracing: inducer of adipogenesis and prolonged nuclear translocation of Cre recombinase. Mol. Metab. *4*, 771–778.

Yoneshiro, T., Aita, S., Matsushita, M., Kayahara, T., Kameya, T., Kawai, Y., Iwanaga, T., and Saito, M. (2013). Recruited brown adipose tissue as an antiobesity agent in humans. J. Clin. Invest. *123*, 3404–3408.

Zhang, Y., Goldman, S., Baerga, R., Zhao, Y., Komatsu, M., and Jin, S. (2009). Adipose-specific deletion of autophagy-related gene 7 (atg7) in mice reveals a role in adipogenesis. Proc. Natl. Acad. Sci. USA *106*, 19860–19865.

Cell Metabolism, Volume *24*

Supplemental Information

Beige Adipocyte Maintenance Is Regulated by Autophagy-Induced Mitochondrial Clearance

Svetlana Altshuler-Keylin, Kosaku Shinoda, Yutaka Hasegawa, Kenji Ikeda, Haemin Hong, Qianqian Kang, Yangyu Yang, Rushika M. Perera, Jayanta Debnath, and Shingo Kajimura

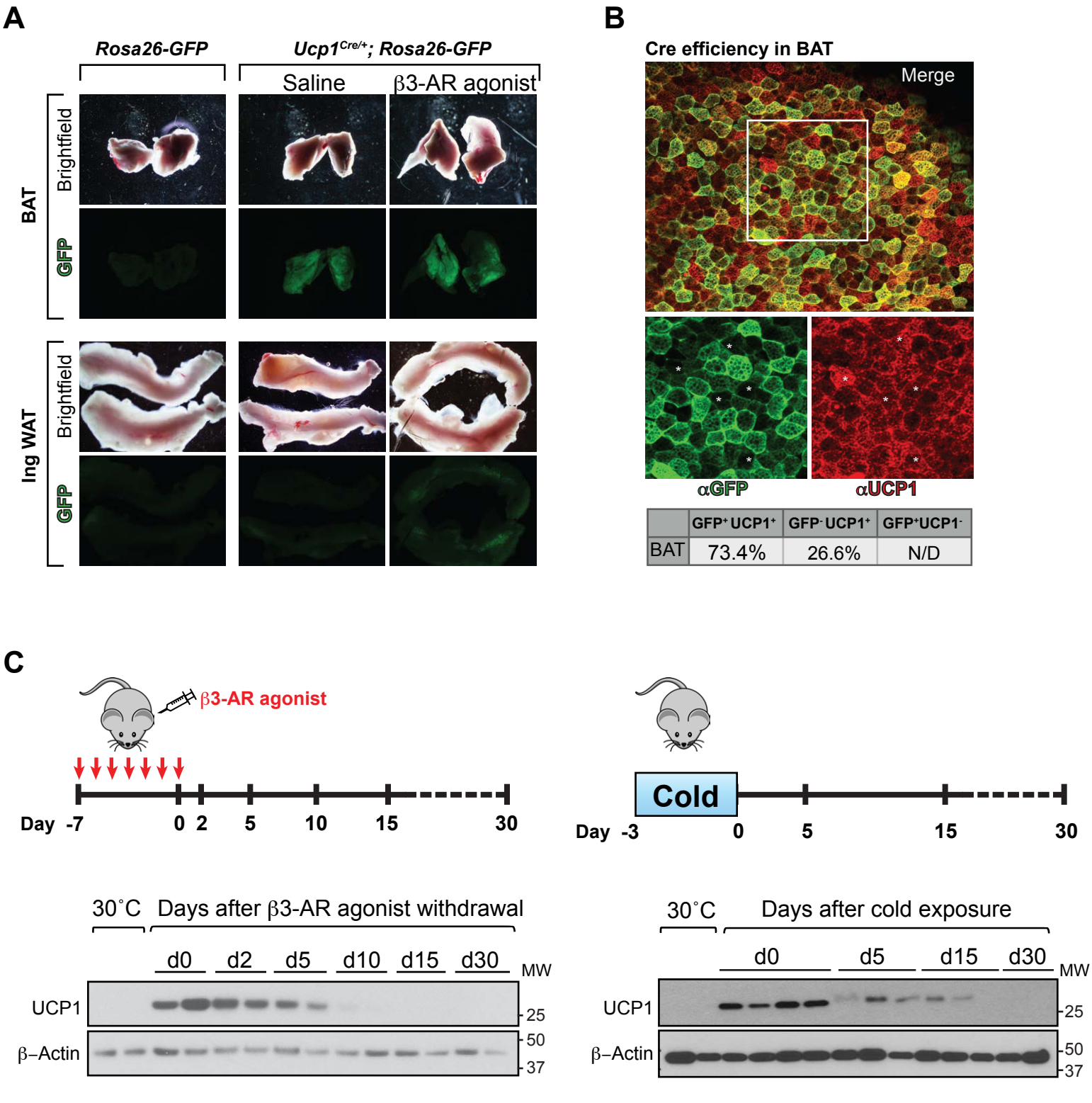

Figure S1: Supplement to Figure 1.

A

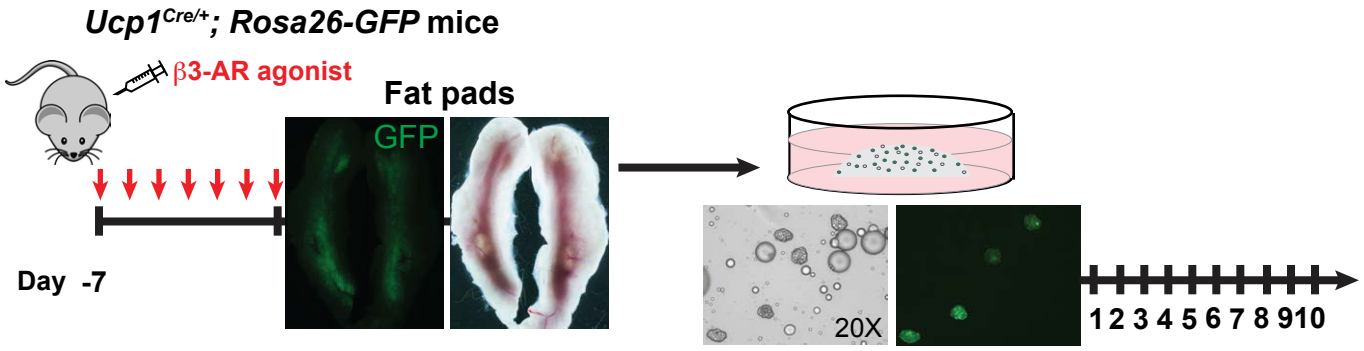

B

Stage	Morphology	Description
Stage I	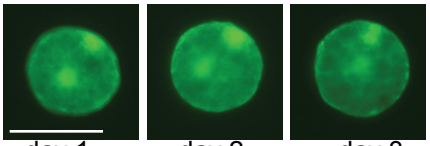 day 1 day 2 day 3	Innumerous,dense lipid dropplets
Stage II	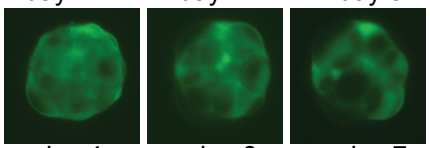 day 4 day 6 day 7	Larger bulging lipid droplets, more than four droplets per plane of view
Stage III	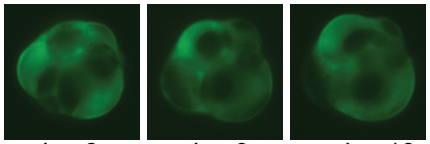 day 8 day 9 day 10	Four or less lipid droplets per plane of view

C

Fibroblast-like	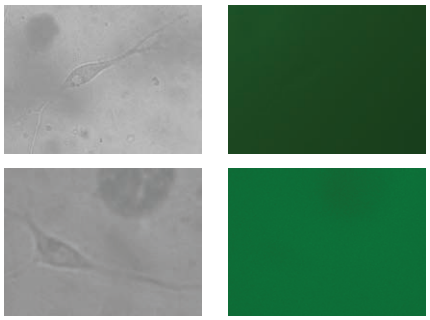	Elongated; with cellular protrusions

D

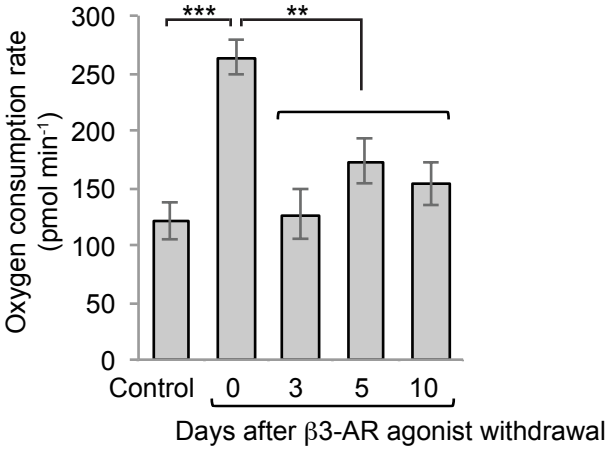

Figure S2: Supplement to Figure 2.

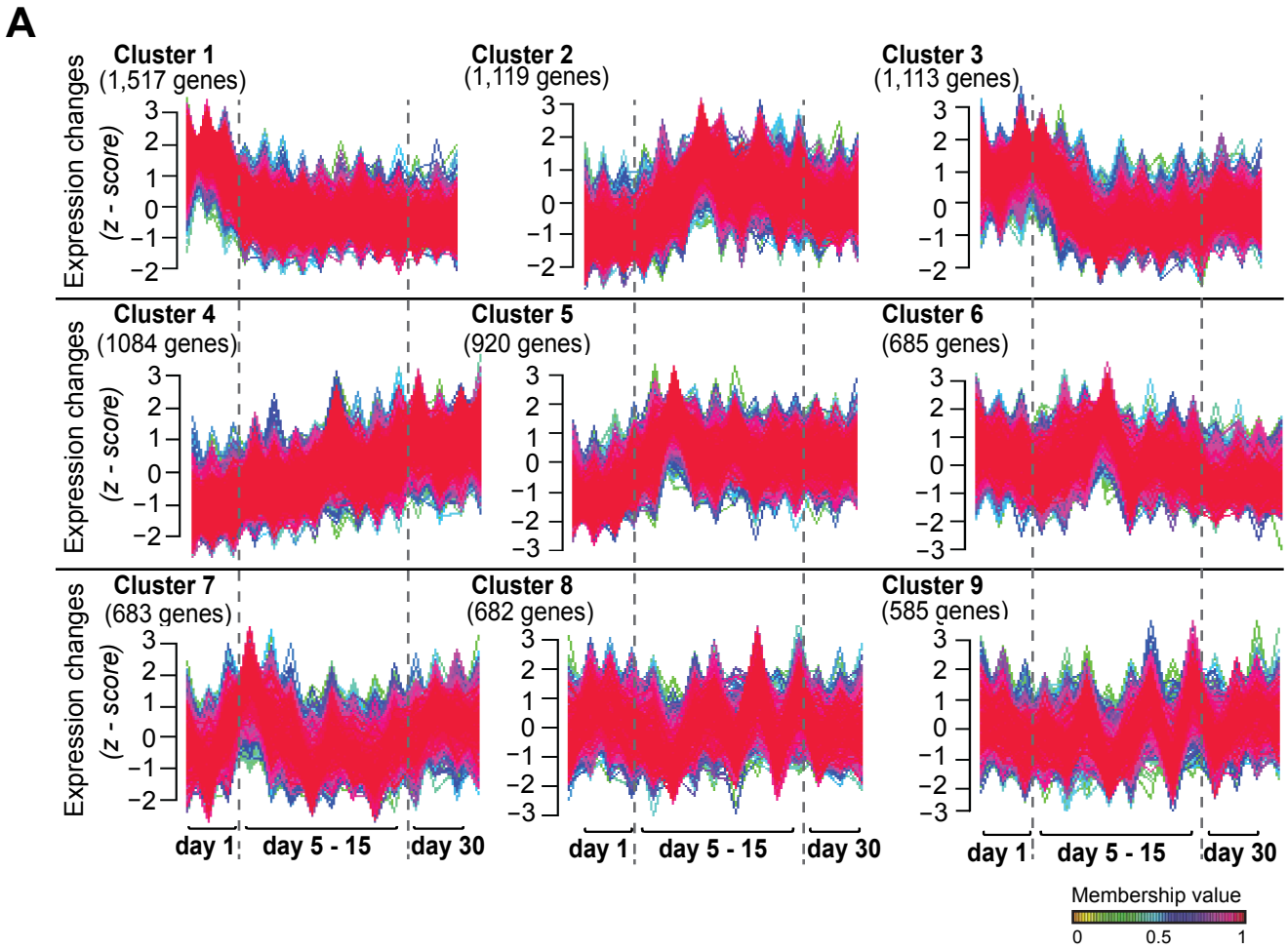

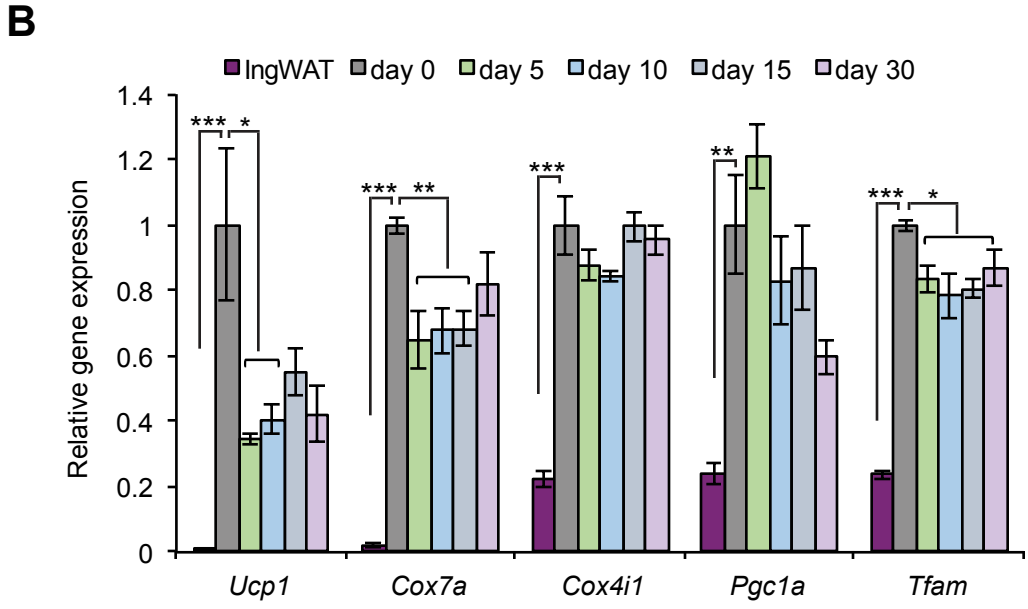

Figure S3: Supplement to Figure 3.

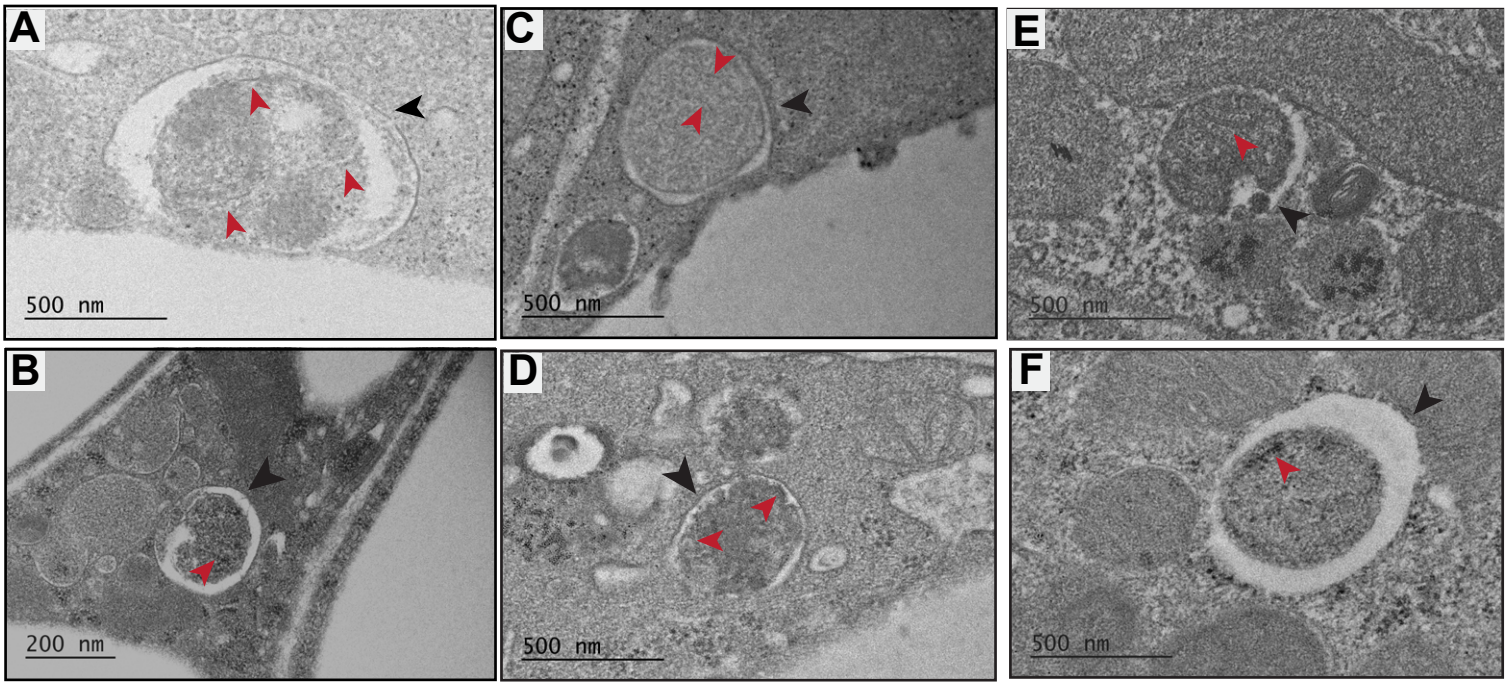

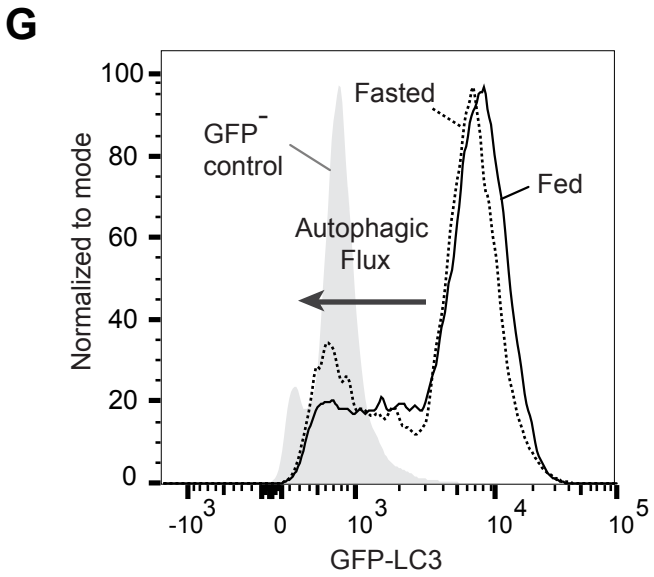

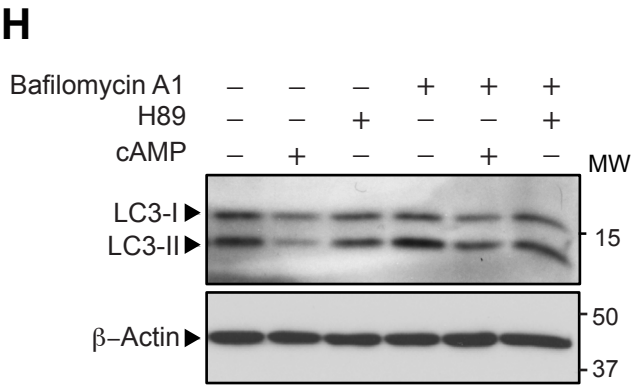

Figure S4: Supplement to Figure 4.

A

De Novo Motif	Known Motif	TF	*P* - value
		FOXO3 (MA0157.2)	1 x 10^{-2}

B

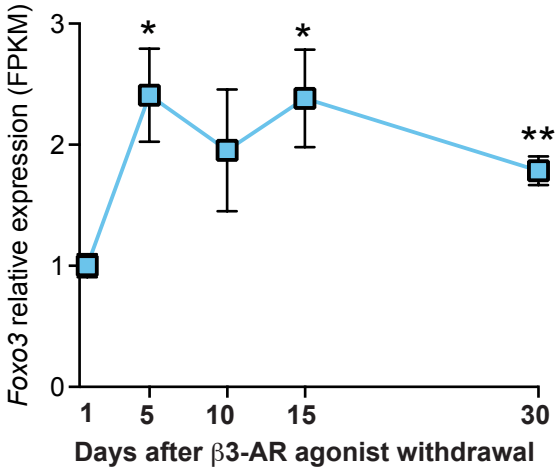

C

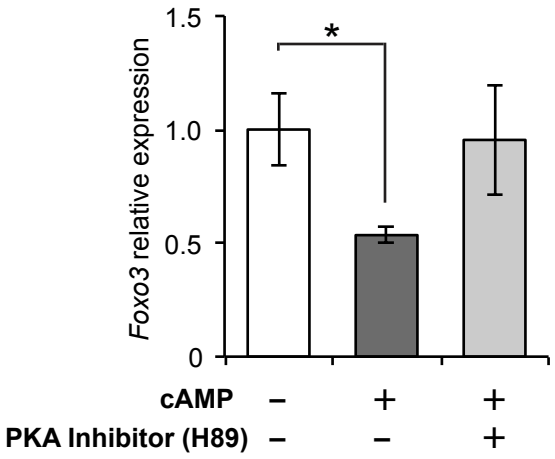

Figure S5: Supplement to Figure 5.

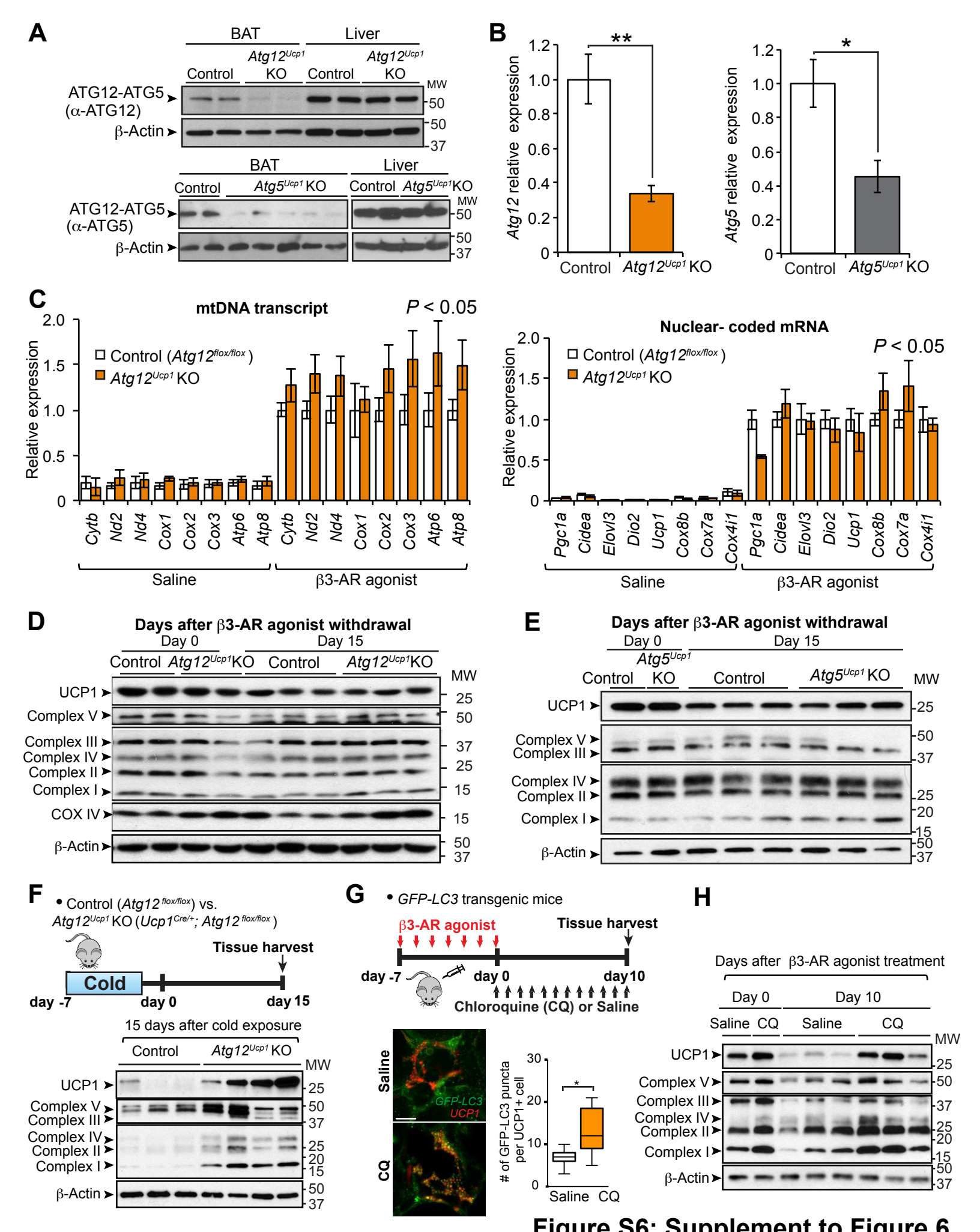

Figure S6: Supplement to Figure 6.

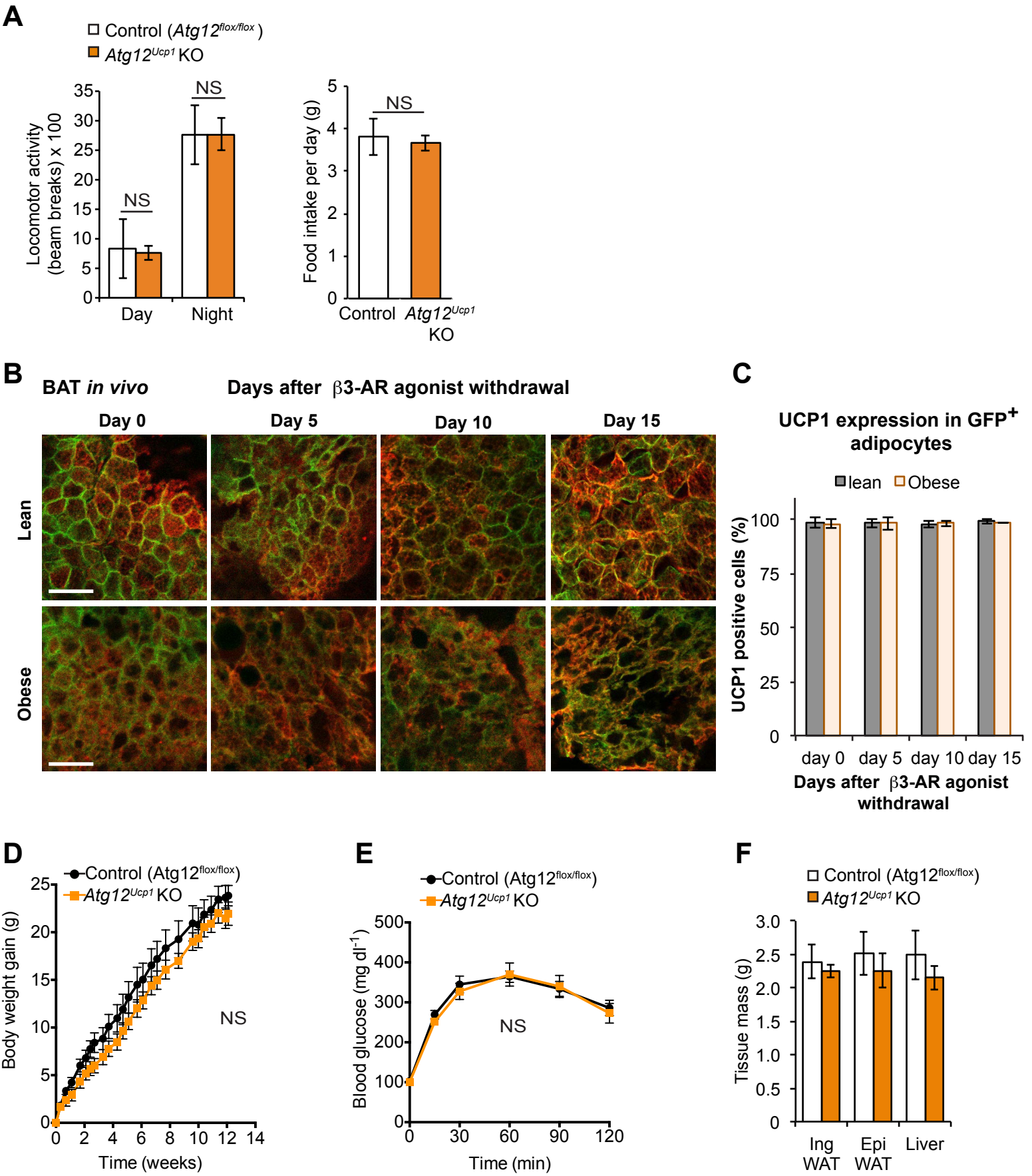

Figure S7: Supplement to Figure 7.

SUPPLEMENTARY FIGURE LEGENDS

Figure S1: Supplement to Figure 1.

Experimental system to monitor beige adipocytes in vivo.

(**A**) Endogenous GFP expression in the interscapular BAT and inguinal WAT of control (*Rosa26-GFP)* and *Ucp1$^{Cre/+}$;Rosa26-GFP* reporter mice following treatment with the ß3-AR agonist CL316,243 at 1mg kg^{-1} for seven consecutive days under thermoneutrality (30˚C). Mice were bred and maintained under thermoneutrality. Tissue analysis was carried out immediately after ß3-AR agonist withdrawal (day 0). Note that GFP positive adipocytes were detected in the interscapular BAT in the presence or absence of ß3-AR agonist. In contrast, in the inguinal WAT beige adipocytes emerge only after chronic treatment with ß3-AR agonist. *n* = 3-4.

(**B**) *Cre* efficiency was determined in the interscapular BAT of *Ucp1$^{Cre/+}$;Rosa26-GFP* reporter mice by counting the number of UCP1^{+} cells that did not express GFP. Cre efficiently labeled approximately 73% of UCP1-expressing cells. Note that GFP^{+} cell that did not express UCP1 were not observed (N/D, not detected). *n* = 551. White asterisks are labeling UCP1^{+} GFP^{-} cells.

(**C**) Left panel; Wild-type mice were treated with the ß3-AR agonist CL316,243 at 1mg kg^{-1} for seven consecutive days. Inguinal WAT depots were harvested for molecular analyses at indicated time points following ß3-AR agonist withdrawal. Immunoblotting for UCP1 in the inguinal WAT of mice under thermoneutrality (30˚C) and the inguinal WAT of mice at indicated time points following ß3-AR agonist withdrawal. ß-actin was used as a loading control.

Right panel; Wild-type mice were exposed to cold (6˚C) for three consecutive days. Inguinal WAT depots were harvested for molecular analysis at indicated time-points after acclimation to ambient temperature. Immunoblotting for UCP1 in the inguinal WAT of mice under thermoneutrality (30˚C) and the inguinal WAT of mice at indicated time points after re-warming following cold exposure. ß-actin was used as a loading control. Note that the time-dependent decline in UCP1 expression after acclimation to ambient temperature was similar to the decline found after ß3-AR agonist withdrawal.

Figure S2: Supplement to Figure 2.

Ex vivo system to track morphological and functional changes of beige adipocytes.

(**A**) Schematic illustration to monitor individual beige adipocytes *ex vivo* in response to chronic treatment with ß3-AR agonist CL316,243 at 1mg kg^{-1} for seven days. Inguinal WAT depots from *Ucp1*$^{Cre/+}$*;Rosa26-GFP* mice were isolated immediately after chronic treatment with ß3-AR agonist, digested to single cells, embedded in Collagen I gel, and maintained in a live cell culture for ten consecutive days. Culture medium did not contain any stimuli, such as ß3-AR agonist, that control beige adipocyte differentiation.

(**B**) Morphological changes occurring between day 1-10 of culture were categorized into three stages (Stage I, Stage II, Stage III) based on lipid content *per* plane view.

(**C**) Examples of fibroblast-like cells in *ex vivo* culture. Note that GFP-positive fibroblast-like cells were not observed at any time point of the culture.

(**D**) Basal oxygen consumption rate of the *ex vivo* cultured inguinal WAT from wild-type mice at indicated days after ß3-AR agonist withdrawal. Inguinal WAT depots from wild-

type animals under thermoneutrality were used as a control. ** *P* <0.01, *** *P* <0.001, by two-tailed Student's *t*-test, n = 3 - 6 technical replicates. Data are expressed as means ± s.e.m.

Figure S3: Supplement to Figure 3.

Gene expression profile of beige adipocytes and BAT following β3-AR agonist withdrawal.

(**A**) The Fuzzy C-Means (FCM) clustering was performed to identify gene clusters that exhibited similar expression profiles. The *z*-transformed profiles of beige adipocytes during the beige-to-white transition (day 0–30) underwent the FCM clustering. Color represents the likelihood of a gene belonging to each gene cluster, red (most likely)-blue- yellow (least likely). The identified 9 clusters were numbered from most populated to least populated by gene sets. Cluster I, containing 1517 genes, exhibited the most frequent gene expression profile. Y-axis represents expression changes in the expression level (*z*-scored FPKM) of each gene. The genes for Cluster I are listed in Supplementary Table1.

(**B**) Gene expression profiles of brown/beige-enriched mitochondrial genes (*Ucp1*, *Cox7a* and *Cox4i1*) and key transcriptional regulators of mitochondrial biogenesis (*Pgc1a* and *Tfam*) in the interscapular BAT depots at indicated time points after ß3-AR agonist withdrawal. As a reference, expression levels of each gene in inguinal WAT are shown. * *P* <0.05, ** *P* <0.01, *** *P* <0.001 by two-tailed Student's *t*-test. *n* = 3. Data are expressed as means ± s.e.m.

Figure S4: Supplement to Figure 4.

Evidence of mitophagy in beige adipocytes following β3-AR agonist withdrawal.

(**A - F**) Electron microscopy (EM) images were obtained in beige adipocytes during the transition phase. (**A and B**) Adipocytes at day 5 following ß3-AR agonist withdrawal. (**C and D**) Adipocytes at day 10. (**E and F**) Adipocytes at day 15. Black arrowheads indicate the autophagic vesicles containing mitochondrial remnants, as identified by remaining cristae (red arrowheads).

(**G**) Twenty-four hours of fasting led to a decrease in GFP-LC3 fluorescence, indicating an increase in autophagic flux. Wild-type animal was used as control for GFP fluorescence. X-axis represents GFP-LC3 fluorescence intensity and Y-axis represents the number of adipocytes normalized to mode. Analysis was done using FlowJo software.

(**H**) Immunoblotting for LC3 in primary beige adipocytes following treatments with Bafilomycin A1, cAMP (forskolin), and H89. Differentiated beige adipocytes were treated with forskolin at a dose of 10 μM in the presence and absence of Bafilomycin A1 (50 nM) for 2 hours. The PKA inhibitor H89 at a dose of 10 μM was added 1 hr prior to forskolin treatment.

Figure S5: Supplement to Figure 5.

Regulation of *Foxo3* expression in beige adipocytes.

(A) The HOMER-based motif analysis of lysosomal genes in Figure 5A.

(**B**) Relative expression of *Foxo3* during the beige-to-white adipocyte transition. * *P* <0.05, ** *P* <0.01, by two-tailed Student's *t*-test. *n* = 3. Data are expressed as means ± s.e.m.

(**C**) mRNA expression of *Foxo3* in response to cAMP in the presence or absence of the PKA inhibitor H89. Differentiated beige adipocytes were treated with forskolin (cAMP) at a dose of 10 μM for 4hr in the presence or absence of H89. The PKA inhibitor H89 at a dose of 10 μM was added 1 hr prior to forskolin treatment. * *P* <0.05 by two-tailed Student's *t*-test. *n* = 3. Data are expressed as means ± s.e.m.

Figure S6: Supplement to Figure 6.

Molecular characterization of the interscapular BAT and inguinal WAT depots in *Atg12*^{Ucp1} KO mice and *Atg5*^{Ucp1} KO mice.

(**A**) Immmunoblotting for the ATG12-ATG5 complex in the interscapular BAT and liver of control (*Atg12*$^{flox/flox}$) and *Atg12*^{Ucp1} KO (*Ucp1*$^{Cre/+}$;*Atg12*$^{flox/flox}$) mice (left) or control (*Atg5*$^{flox/flox}$) and *Atg5*^{Ucp1} KO (*Ucp1*$^{Cre/+}$;*Atg5*$^{flox/flox}$) mice (right). ß-actin was used as a loading control. Molecular weight (MW) is shown on the right.

(**B**) Left panel; *Atg12* mRNA levels in beige adipocytes from control and *Atg12*^{Ucp1}KO mice. Beige adipocytes were isolated by FACS from control (*Ucp1*$^{Cre/+}$*; Rosa26-GFP)* and *Atg12*^{Ucp1}KO (*Ucp1*$^{Cre/+;}$*Atg12*$^{flox/flox}$*;Rosa26-RFP)* mice following 5 days of cold exposure. mRNA expression of *Atg12* was measured by qPCR. *n* = 3-4. Right panel; *Atg5* mRNA levels in beige adipocytes from control and *Atg5*^{Ucp1}KO mice. Beige adipocytes were isolated by FACS from control (*Ucp1*$^{Cre/+}$*; Rosa26-GFP)* and *Atg5*^{Ucp1}KO (*Ucp1*$^{Cre/+;}$*Atg5*$^{flox/flox}$*;Rosa26-RFP)* mice following 5 days of cold exposure.

mRNA expression of *Atg5* was measured by qPCR. * P <0.05 by two-tailed Student's *t*-test. n = 3. Data are expressed as means ± s.e.m.

(**C**) Mitochondrial DNA (mtDNA) transcripts (left panel, as indicated) and mRNA transcript of nuclear-coded beige fat-enriched genes (right panel, as indicated) were quantified in the inguinal WAT depots of control ($Atg12^{flox/flox}$) and $Atg12^{Ucp1}$ KO mice chronically treated with saline or ß3-AR agonist for seven consecutive days. n = 4. Data are expressed as means ± s.e.m. Expression of all the indicated genes was significantly increased in the Inguinal WAT of ß3-AR agonist treated mice, as compared to saline-treated mice (P < 0.05).

(**D**) Immunoblotting for UCP1 and mitochondrial complexes (as indicated) in the interscapular BAT of control ($Atg12^{flox/flox}$) and $Atg12^{Ucp1}$ KO ($Ucp1^{Cre/+;}Atg12^{flox/flox}$) mice at day 0 and day 15 following ß3-AR agonist withdrawal. ß-actin was used as a loading control. Molecular weight (MW) is shown on the right.

(**E**) Immunoblotting for UCP1 and mitochondrial complexes (as indicated) in the interscapular BAT of control ($Atg5^{flox/flox}$) and $Atg5^{Ucp1}$ KO ($Ucp1^{Cre/+;}Atg5^{flox/flox}$) mice at day 0 and day 15 following ß3-AR agonist withdrawal. ß-actin was used as a loading control. Molecular weight (MW) is shown on the right.

(**F**) Top panel; control ($Atg12^{flox/flox}$) and $Atg12^{Ucp1}$ KO mice were housed at 6˚C for 7 days and subsequently kept at room temperature for 15 days. Inguinal WAT depots were harvested for molecular analysis. Bottom panel; immunoblotting for UCP1 and mitochondrial complexes (as indicated) in the Inguinal WAT of control ($Atg12^{flox/flox}$) and $Atg12^{Ucp1}$ KO ($Ucp1^{Cre/+;}Atg12^{flox/flox}$) mice at day 15 after cold exposure. ß-actin was used as a loading control. Molecular weight (MW) is shown on the right.

(**G**) Top panel; *GFP-LC3* mice were treated with ß3-AR agonist for 7 days. Subsequently, the mice were treated with chloroquine (CQ) at a dose of 60 mg kg^{-1} or saline daily for 10 days following ß3-AR agonist withdrawal. Inguinal WAT depots were harvested for molecular analysis. Bottom panel; confocal images of beige adipocytes from *GFP-LC3* mice after saline or chloroquine (CQ) treatment. UCP1+ beige adipocytes and LC3 were visualized by immunohistochemistry for UCP1 (red) and GFP (green), respectively. Quantification of GFP+ LC3 puncta per UCP1+ cell is shown.

(**H**) Immunoblotting for UCP1 and mitochondrial complexes (as indicated) in the Inguinal WAT of *LC3-GFP* mice treated with saline or chloroquine (CQ) daily for 10 days following ß3-AR agonist withdrawal. ß-actin was used as a loading control. Molecular weight (MW) is shown on the right.

Figure S7: Supplement to Figure 7.

Metabolic phenotype of *Atg12^{Ucp1}* KO mice.

(**A**) Left panel; locomotor activity (beam breaks) in control (*Atg12$^{flox/flox}$*) and *Atg12^{Ucp1}* KO (*Ucp1$^{Cre/+;}$Atg12$^{flox/flox}$*) mice measured using CLAMS under a regular diet. n = 6. N.S., not significant. Right panel; food intake was measured in control and *Atg12^{Ucp1}* KO mice under a high-fat diet for 2.5 weeks. N.S., not significant. n = 6-7.

(**B**) Confocal images of fixed interscapular BAT sections from *Ucp1$^{Cre/+;}$mT/mG* reporter mice under a regular diet (top panel, lean) and age-matched obese mice under a high-fat diet (bottom panel, obese). Cellular membrane of brown adipocytes was visualized by membrane-targeted GFP (mGFP, Green). Endogenous UCP1 was mimmunostained (Red). Scale bar, 57μm.

(**C**) Quantification of mGFP-positive adipocytes in lean and obese mice that express endogenous UCP1 in (A). n = 100 cells or more per group.

(**D**) Body weight gain of control (*Atg12*$^{flox/flox}$) and *Atg12*^{Ucp1} KO mice under a high-fat diet without ß3-AR agonist treatment. Control and *Atg12*^{Ucp1} KO mice were fed a high-fat diet for 12 weeks. Body weight was measured twice a week. *n* = 6-7 per genotype. N.S., not significant. Data are expressed as means ± s.e.m.

(**E**) After 12 weeks of high-fat diet, control and *Atg12*^{Ucp1} KO mice from (A) were fasted for 12 hours and injected with 1.5g kg^{-1} glucose. Whole-body glucose was measured at 15, 30, 60, 90, and 120 min. N.S., not significant. Data are expressed as means ± s.e.m.

(**F**) Tissue weight of inguinal WAT, epididymal WAT, and liver from control and *Atg12*^{Ucp1} KO mice from (A). N.S., not significant. Data are expressed as means ± s.e.m.

EXPERIMENTAL PROCEDURES

Animals. All animal experiments were performed under the guidelines established by the UCSF Institutional Animal Care and Use Committee. Unless otherwise specified, all mice used for the experiments are 8-12 weeks old males on C57BL/6 background. *Ucp1*$^{Cre/+}$ mice (Kong et al., 2014) and *Adiponectin*$^{Cre/+}$ mice (Eguchi et al., 2011) were kindly provided by Dr. Evan Rosen in Beth Israel Deaconess Medical Center and Harvard Medical School. *GFP-LC3* mice (Mizushima et al., 2004) and *Atg5* $^{flox/flox}$ mice (Hara et al., 2006) were kindly provided by Dr. Noboru Mizushima at the University of Tokyo, graduate school and faculty of medicine. *Atg12*$^{flox/flox}$ mice were recently described (Malhotra et al., 2015). To visualize brown and beige adipocytes *in vivo*, *Ucp1*$^{Cre/+}$ mice were crossed with Rosa26-GFP or mT/mG mice that were obtained from the Jackson Laboratory. To induce beige adipocyte biogenesis, the ß3-AR agonist CL316,243 (Sigma, C5976) was administered intraperitoneally to male mice at a dose of 1mg kg^{-1} for seven consecutive days. To assess the basal amount of GFP-positive cells present in adipose tissues prior to ß3-AR agonist treatment, mice were bred and treated with ß3-AR agonist at thermoneutrality (30 ˚C). For cold exposure experiments, animals were single-caged and exposed to 6 ˚C for five to seven days. For starvation experiments, mice were deprived of food for 24 hours while maintaining access to water. To examine whether the beige-to-white adipocyte transition is altered under obesity, *Ucp1*$^{Cre/+}$*; mT/mG* reporter mice were fed under a regular diet or high-fat diet for 12 weeks. For pharmacological inhibition of autophagy, the anti-malarial chloroquine

(Sigma, C6628) was administered daily by intraperitoneal injection at 60 mg kg^{-1} for up to 15 days following ß3-AR agonist withdrawal.

***Ex vivo* monitoring of beige and brown adipocytes.** Mature adipocytes from the inguinal WAT and interscapular BAT depots of CL316,243-treated *Ucp1$^{Cre/+}$;Rosa26-GFP* mice were isolated by fractionation, embedded in collagen gel containing 2.5 mg ml^{-1} Collagen I (BD354236), 1 µg ml^{-1} Fibronectin (Millipore, FC010), and 0.1% BSA. The cell-containing gel was allowed to solidify at 37˚C for 30 min and cultured in DMEM supplemented with 10% FBS. Culture medium did not contain any stimuli, such as ß3-AR agonist, that control beige adipocyte differentiation. Individual live GFP^+ adipocytes were traced daily for ten consecutive days using the In Cell Analyzer 2000 to define and re-image the position of interest over time. Images were processed using In Cell Developer Toolbox V1.8 (GE Healthcare Life Sciences) and Volocity 6.1.1 software (Improvision).

Immunofluorescence microscopy. For whole-mount immunofluorescence, interscapular BAT and inguinal WAT depots were harvested, chopped into 3-5mm pieces, fixed in 4% paraformaldehyde overnight at 4˚C, blocked in PBS containing 5% goat serum, 1% BSA, and 0.5% Tween20, and immunostained for UCP1 (1:200, abcam, ab10983) and GFP (1:300, Aves Labs, GFP-1020). All fluorescence-conjugated secondary antibodies were purchased from Invitrogen (1:500 dilution). Subsequently, the tissues were serially dehydrated, cleared with Methyl Salicylate and imaged using the inverted Leica TCS SP5 confocal microscope. To assess GFP-LC3 puncta, the inguinal WAT depots from *GFP-LC3* mice were fixed in 4% paraformaldehyde overnight,

cryopreserved in 30% sucrose in PBS at 4˚C overnight, embedded in OCT, and cryo-sectioned at 18 μm. Wild-type mice were used as a control to confirm the specificity of GFP signal. Slides were blocked in PBS containing 5% goat serum, 0.2% BSA, and 0.1% Tween20, stained overnight for GFP and Tom20 (1:100, SCBT, sc-11415) at 4 ˚C. The slides were stained with secondary antibodies for one hour at room temperature, and mounted in Vectashield (Vector Labs). Imaging was done using the aforementioned confocal microscope. To assess adipocyte morphology and UCP1 expression under in obese or lean mice, tissues were fixed in 4% paraformaldehyde for 30min at room temperature (RT), cryopreserved in 30% sucrose in PBS at 4˚C overnight, embedded in OCT, and cryosectioned at 100 μm. Slides were post-fixed with 4% paraformaldehyde for 15 min (RT), blocked in PBS containing 5% goat serum, 0.2% BSA, and 0.1% Tween20, stained overnight for UCP1 (1:200). mGFP and UCP1 expression were visualized by confocal microscopy.

Optical clearing of adipose tissues. BAT and inguinal WAT depots were cut into 3-5mm pieces, immediately fixed in 4% PFA overnight at 4˚C, washed with PBS, dehydrated using serial ethanol washes, and then incubated in methyl salicylate (Sigma) for 30 min. Brightfield images were obtained using Olympus MVX10 stereomicroscope. All imaging analysis was carried out using Volocity 6.1.1 (Improvision) acquisition software.

Transmission electron microscopy. Adipose tissues were fixed in PBS, containing 2.0% electron microscopy grade glutaraldehyde and 2.5% formaldehyde, and

immediately minced to 1 mm cubes. The adipose tissue samples were processed at the Diabetes Center (UCSF) electron microscopy core facility for standard transmission electron microscopy processing and imaging using JEOL 1400 transmission electron microscope.

Flow Cytometry. To isolate GFP-positive adipocytes, inguinal WAT depots from *Ucp1$^{Cre/+}$;Rosa26-GFP* or Adiponectin$^{Cre/+}$*;Rosa26-GFP* mice were digested to single cells using Collagenase D (1.5 U ml^{-1}) and Dispase II (2.5 U ml^{-1}).). Adipocytes were first gated based on size and granularity. Dead cells were removed based on Sytox Blue (1:400) staining. GFP-positive cells were gated based on GFP-negative control cells from wild-type mice not expressing GFP. The same sorting strategy was used to isolate RFP-positive adipocytes from *Ucp1$^{Cre/+;}$Atg12$^{flox/flox}$;Rosa26-LSL-RFP* and *Ucp1$^{Cre/+;}$Atg5$^{flox/flox}$;Rosa26-LSL-RFP* mice. Preadipocytes were isolated from the stromal vascular fraction of wild-type mice using the cell surface markers (Lin^{-} /CD29^{+}/CD34^{+}/Sca1^{+}) that were previously described (Rodeheffer et al., 2008). The following antibodies were used for the isolation of preadipocytes: Sca-1-PB (1:800, Biolegend 108120), CD45-PE (1:200, eBioscience, 12-0451-82), CD31-PE (1:300, bdbiosciences, 553373), CD11b-PE-Cy7 (1:3000 eBiescience), CD29-Alexa700 (1:400 Biolegend, 102218), CD34-FITC (1:25, eBioscience, 11-0341-85), Ter119-PE (1:200, Biolegend, 116207), Sytox Red (1:1000) in 4% BSA in PBS. All the cells were isolated into Trizol LS using FACS Aria II (Becton Dickinson) equipped with 130 μm nozzle diameter for adipocytes or 100 μm for preadipocytes. To monitor autophagic flux in *GFP-LC3* mice *in vivo*, adipocyte fractions were analyzed for GFP using FACS LSR II

(Becton Dickinson), as described previously (Warr et al., 2013). As a positive control for autophagic flux quantification, the GFP-LC3 signal was monitored in the inguinal WAT of *GFP-LC3* mice. The mice were under a fed state or fasted state for 24 hours to induce autophagy (Mizushima et al., 2004). FlowJo software was used for data analysis.

RNA-sequencing. Total RNA was extracted from FACS-isolated GFP-positive adipocytes or preadipocytes using the RNeasy Micro Kit (Qiagen). RNA quality (RIN: RNA Integrity Number) was determined by Bioanalyzer (Agilent Technologies) and samples with RIN of >7.0 were subjected to RNA-sequencing. Libraries were constructed from minimum of 22 ng of total RNA as previously described (Shinoda et al., 2015). High-throughput sequencing was performed using a HiSeq 2500 instrument (Illumina) at the UCSF Institute for Human Genetics core facility. Quality control check on the raw sequence data was done by FastQC (The Babraham Bioinformatics). Raw sequences were mapped using TopHat version 2.0.8 against the mouse (version: mm10) genome. The mapped sequences were converted to FPKM (fragments per kilobase of exon per million fragments mapped) by running Cuffdiff 2.1.1 (Trapnell et al., 2013) to determine gene expression. Reproducibility of the RNA-sequencing data was confirmed by sequencing the identical RNA-samples (R^2 = 0.983). The data were deposited in ArrayExpress (http://www.ebi.ac.uk/arrayexpress/) under accession numbers E-MTAB-3978. RNA-sequencing dataset of the inguinal WAT from mice kept under ambient temperature and 4˚C cold for 5 days has been described previously (Shinoda et al., 2015) and analyzed by the pseudoalignment-based quantification program, kallisto (Bray et al., 2016).

Multivariate Statistics. Clustering of genes was performed as follows: the FPKM profiles of genes at several time points (day 0 - 30 of ß3-AR agonist withdrawal) were *z*-transformed, as such, the mean for each gene was zero and standard deviation was one. The Fuzzy C-Means (FCM) clustering analysis was described elsewhere (Olsen et al., 2006). Subsequently, the *z*-transformed expression profiles were clustered based on the FCM clustering algorithm implemented in Mfuzz toolbox (Futschik and Carlisle, 2005). The top 10,000 highly expressed genes were used for the clustering. The FCM parameters were c = 9 and m = 1.15, respectively. For principal component analysis (PCA), preadipocytes ($Lin^-/CD29^+/CD34^+/Sca1^+$) and white adipocytes (*Adiponectin* $^{Cre/+}$;*Rosa26-GFP*) were first mapped onto two-dimensional (PC1 and PC2) space, based on the expression of 10,138 genes that showed differences between the two groups by 2-fold or more. Subsequently, the transcriptome of GFP-positive adipocytes at each time point (day 0-30) was mapped on the same PC plot, based on the expression levels of 10,138 genes. Similar PC plots were reproducibly found when different number of genes (2,000, 1,000, or 500) were applied. Above statistical analyses were performed using the JMP software version 11 (SAS Institute) or Multi Experiment Viewer (MeV) (Saeed et al., 2003). Gene Ontology (GO) enrichment analysis was performed in DAVID (Huang et al., 2009) using the biological process and cellular component terms. Transcription factor binding motif analysis was performed by Hypergeometric Optimization of Motif EnRichment analysis (HOMER) (Heinz et al., 2010).

Cell culture. Beige adipocyte differentiation was induced in primary preadipocytes from inguinal WAT by treating with DMEM/F12 medium containing 10% FBS, 0.5 mM isobutylmethylxanthine, 125 nM indomethacin, 2 μg ml^{-1} dexamethasone, 850 nM insulin, and 1 nM T3, and 0.5 μM Rosiglitazone. Two days after induction, cells were switched to the maintenance medium containing 10% FBS, 850 nM insulin, 1 nM T3, and 0.5 μM Rosiglitazone for 7 days. Cells were then pretreated with 10 μM H89 (Cayman chemical) for 1 hour followed by 4 hour treatment with 10 μM Forskolin. Bafilomycin A1 at a dose of 50 nM was used for the assessment of autophagy flux in beige adipocytes. To induce a fasted condition in culture, differentiated beige adipocytes were cultured in amino acid-free, glucose-free RPMI-1640 (US Biological, Inc., R9010-02) supplemented with 10% dialyzed FBS (Sigma, F0392) for 8 hours.

Mitochondrial respiration assays. Oxygen consumption rate (OCR) in the inguinal WAT and interscapular BAT was measured using the Seahorse XFe Extracellular Flux Analyzer. The adipose tissues (1.5 mg) were placed into XF24 Islet Capture Microplates (Seahorse Bioscience) and pre-incubated for one hour with assay media in the presence or absence of 5 μM isoproterenol (Sigma I6504-500MG) to induce cAMP-dependent respiration. For *ex vivo* culture experiments, inguinal WAT depots were isolated from wild-type mice treated with 7-day β3-AR agonist and maintained in DMEM (10-017-CV) supplemented with 10% FBS for 3, 5, and 10 days after β3-AR agonist withdrawal. The XF assay medium was supplemented with 1 mM sodium pyruvate, 2 mM GlutaMAX™-I, and 25 mM glucose. Tissues were subjected to the mitochondrial stress test by adding 10 μM oligomycin (Cell Signaling; 9996), followed by 20 μM

carbonyl cyanide 4-(trifluoromethoxy) phenylhydrazone (FCCP) (Sigma, C2920-10MG) and 20 μM antimycin (Sigma, A8674-50MG).

Metabolic studies. To assess whole-body energy expenditures, 10-week-old *Atg12*$^{Ucp1\ KO}$ mice (*Ucp1*$^{Cre/+}$;*Atg12*$^{flox/flox}$) and body-weight-matched littermate control mice (*Atg12* $^{flox/flox}$) were treated with β3-AR agonist for 7 days and maintained at thermoneutrality during β3-AR agonist withdrawal. Whole-body energy expenditure was measured between 17 and 18 days after β3-AR agonist withdrawal using a Comprehensive Lab Animal Monitoring System (CLAMS, Columbus Instruments). Locomotor activity was simultaneously monitored by the CLAMS. For diet-induced obesity study, 9-week-old *Atg12*$^{Ucp1\ KO}$ and control (*Atg12* $^{flox/flox}$) male mice were fed a high-fat diet (HFD) (60% kcal%, D12492, Research Diet Inc.). Following seven-day β3-AR agonist treatment, mice were transferred to thermoneutrality (30 ˚C) for 8 weeks. Body weight was measured twice per week. Glucose tolerance test experiments were performed at 8 weeks or 12 weeks of high-fat diet, as indicated. After an overnight fast, the mice were injected intraperitoneally with 1.5 g kg^{-1} glucose. Insulin tolerance test was performed after 8.5 weeks of high-fat diet. After a 3 hour fast, mice were injected intraperitoneally with 0.75 U kg^{-1} Insulin (Novolin). Blood samples were collected at indicated time points and amounts of glucose were measured using blood glucose test strips (FreeStyle Lite).

RNA Preparation and Quantitative PCR. Total RNA was extracted from inguinal WAT depots using Trizol followed by the RNeasy mini-kit (Qiagen). Gene expression analysis

of adipose tissues was carried out as detailed elsewhere (Sharp et al., 2012). The primer sequences are listed in **Supplementary Table 2.**

Immunoblotting. Protein lysates from adipose tissues was extracted using Qiagen TissueLyzer LT and RIPA buffer containing 50 mM Tris, pH 7.5, 150 mM NaCl, 1% Triton-X, 10% glycerol, and cOmplete protease inhibitors (Roche). For monitoring autophagy, the adipocyte fraction from inguinal WAT depots was isolated and applied for immunoblotting. The following antibodies were used in immunoblotting; UCP1 (1:1000, abcam, ab10983), MitoProfile® total OXPHOS rodent antibody cocktail (1:1000, abcam, ab110413), β–actin (1:10,000, Sigma, A3854), ATG12 (1:1000, Cell Signaling, 4180S), ATG5 (1:1000, Cell Signaling, 12994S), NBR1 (1:1000, Novus Bio, NBP1-71703), p62/SQSTM1 (1:1000, Novus Bio, H00008878-M01), LC3 (1:1000, Cell Signaling, 12741S), and COX IV (1:000, Cell Signaling, 4850).

Statistical analyses. Unpaired Student's *t*-test was applied to determine the statistical difference, except for the following analyses: unpaired two-tailed Mann-Whitney U test was applied to compare LC3 puncta at different stages of beige-to-white transition; two-way repeated-measures ANOVA followed by Fisher's LSD test were applied to determine the statistical difference in body weight gain. *P* values below 0.05 were considered significant throughout the study.

Reference

Bray, N.L., Pimentel, H., Melsted, P., and Pachter, L. (2016). Near-optimal probabilistic RNA-seq quantification. Nat Biotechnol *34*, 525-527.

Eguchi, J., Wang, X., Yu, S., Kershaw, E.E., Chiu, P.C., Dushay, J., Estall, J.L., Klein, U., Maratos-Flier, E., and Rosen, E.D. (2011). Transcriptional control of adipose lipid handling by IRF4. Cell metabolism *13*, 249-259.

Futschik, M.E., and Carlisle, B. (2005). Noise-robust soft clustering of gene expression time-course data. Journal of bioinformatics and computational biology *3*, 965-988.

Hara, T., Nakamura, K., Matsui, M., Yamamoto, A., Nakahara, Y., Suzuki-Migishima, R., Yokoyama, M., Mishima, K., Saito, I., Okano, H., et al. (2006). Suppression of basal autophagy in neural cells causes neurodegenerative disease in mice. Nature *441*, 885-889.

Heinz, S., Benner, C., Spann, N., Bertolino, E., Lin, Y.C., Laslo, P., Cheng, J.X., Murre, C., Singh, H., and Glass, C.K. (2010). Simple combinations of lineage-determining transcription factors prime cis-regulatory elements required for macrophage and B cell identities. Molecular cell *38*, 576-589.

Huang, d.W., Sherman, B.T., and Lempicki, R.A. (2009). Systematic and integrative analysis of large gene lists using DAVID bioinformatics resources. Nature protocols *4*, 44-57.

Kong, X., Banks, A., Liu, T., Kazak, L., Rao, R.R., Cohen, P., Wang, X., Yu, S., Lo, J.C., Tseng, Y.H., et al. (2014). IRF4 is a key thermogenic transcriptional partner of PGC-1alpha. Cell *158*, 69-83.

Malhotra, R., Warne, J.P., Salas, E., Xu, A.W., and Debnath, J. (2015). Loss of Atg12, but not Atg5, in pro-opiomelanocortin neurons exacerbates diet-induced obesity. Autophagy *11*, 145-154.

Mizushima, N., Yamamoto, A., Matsui, M., Yoshimori, T., and Ohsumi, Y. (2004). In vivo analysis of autophagy in response to nutrient starvation using transgenic mice expressing a fluorescent autophagosome marker. Molecular biology of the cell *15*, 1101-1111.

Olsen, J.V., Blagoev, B., Gnad, F., Macek, B., Kumar, C., Mortensen, P., and Mann, M. (2006). Global, in vivo, and site-specific phosphorylation dynamics in signaling networks. Cell *127*, 635-648.

Rodeheffer, M.S., Birsoy, K., and Friedman, J.M. (2008). Identification of white adipocyte progenitor cells in vivo. Cell *135*, 240-249.

Saeed, A.I., Sharov, V., White, J., Li, J., Liang, W., Bhagabati, N., Braisted, J., Klapa, M., Currier, T., Thiagarajan, M., et al. (2003). TM4: a free, open-source system for microarray data management and analysis. BioTechniques *34*, 374-378.

Sharp, L.Z., Shinoda, K., Ohno, H., Scheel, D.W., Tomoda, E., Ruiz, L., Hu, H., Wang, L., Pavlova, Z., Gilsanz, V., et al. (2012). Human BAT possesses molecular signatures that resemble beige/brite cells. PloS one *7*, e49452.

Shinoda, K., Luijten, I.H., Hasegawa, Y., Hong, H., Sonne, S.B., Kim, M., Xue, R., Chondronikola, M., Cypess, A.M., Tseng, Y.H., et al. (2015). Genetic and functional characterization of clonally derived adult human brown adipocytes. Nature medicine *21*, 389-394.

Trapnell, C., Hendrickson, D.G., Sauvageau, M., Goff, L., Rinn, J.L., and Pachter, L. (2013). Differential analysis of gene regulation at transcript resolution with RNA-seq. Nature biotechnology *31*, 46-53.

Warr, M.R., Binnewies, M., Flach, J., Reynaud, D., Garg, T., Malhotra, R., Debnath, J., and Passegue, E. (2013). FOXO3A directs a protective autophagy program in haematopoietic stem cells. Nature *494*, 323-327.

Supplementary Table 2. qRT-PCR primers Related to Figure. 5

Gene Name	Forward (5' to 3')	Reverse (5' to 3')
Ahnak	ACACTGTTGGCTTGAAGTTGC	CTGGGCCATCATGCAGATTGT
Atg12	TGTGAATCAGTCCTTTGCCCC	TGCAGGACCAGTTTACCATCAC
Atg4c	GCATCCGGATTTGCAAGGGC	CTCCAGCTGTCACGGAGTCA
Atg5	ATGCGGTTGAGGCTCACTTTA	GGTTGATGGCCCAAAACTGG
Atp6	TGGCATTAGCAGTCCGGCTT	ATGGTAGCTGTTGGTGGGCT
Atp8	TTCCCACTGGCACCTTCACC	TGTTGGGGTAATGAATGAGGCAA
Bnip3	TCCTGGGTAGAACTGCACTTC	GCTGGGCATCCAACAGTATTT
Bnip3l	TGTCTCACTTAGTCGAGCCGC	TGGGTAGCTCCACCCAGGAA
Cidea	ATCACAACTGGCCTGGTTACG	TACTACCCGGTGTCCATTTCT
Cln3	CCCTCGGTTGGATAGTCGGA	GCCTGGTTCCACATGGCTC
Cox1	TAGCCCATGCAGGAGCATCA	TGGCTGGGGGTTTCATGTTGA
Cox2	ACCTGGTGAACTACGACTGCT	CCTAGGGAGGGGACTGCTCA
Cox3	CTTCACCATCCTCCAAGCTTCA	AGTCCATGGAATCCAGTAGCCAT
Cox4i1	GCCTGATTGGCAAGAGAGCC	CAAGGGGTAGTCACGCCGAT
Cox7a	CAGCGTCATGGTCAGTCTGT	AGAAAACCGTGTGGCAGAGA
Cox8b	GAACCATGAAGCCAACGACT	GCGAAGTTCACAGTGGTTCC
Ctns	ATGAGGAGGAATTGGCTGCTT	ACGTTGGTTGAACTGCCATTTT
Ctsa	CAGCCCTCTTTCCGGCAATA	TTTGGGTCGTTCTGCGACTC
Ctsc	TGCCACATCTGAGGAACAAA	CACCAGGACTCCTCTGCATT
Ctsc	TGCCACATCTGAGGAACAAA	CACCAGGACTCCTCTGCATT
Ctsd	GCTTCCGGTCTTTGACAACCT	CACCAAGCATTAGTTCTCCTCC
Cytb	CCTTCATGTCGGACGAGGCTT	TGCTGTGGCTATGACTGCGAA
Dio2	CAGTGTGGTGCACGTCTCCAATC	TGAACCAAAGTTGACCACCAG
Elovl3	TCCGCGTTCTCATGTAGGTCT	GGACCTGATGCAACCCTATGA
Foxo3	AACGGCTCACTTTGTCCCAGA	ACAGGTTGTGCCGGATGGAG
Gm2a	ACTGCTCCTCAGAAGGTGGA	CTTCCTTGAAGGGACAGTGG
Hexb	CTCTTTCGGGACTTTCACCA	CCATGGCATCCAGAGTTTTT
Mcoln1	CTGACCCCCAATCCTGGGTAT	GGCCCGGAACTTGTCACAT
Mitf	AAGTCGGGGAGGAGTTTCACG	GGAGCTTAACGGAGGCTTGGA
Naga	AGAGAACGTGCAGAGGGGTA	TGGACAGCACACTCTTCCAG
Nd2	GCCTGGAATTCAGCCTACTAGC	GGCTGTTGCTTGTGTGACGA
Nd4	CGCCTACTCCTCAGTTAGCCA	TGATGTGAGGCCATGTGCGA
Pgc1a	AGCCGTGACCACTGACAACGAG	GCTGCATGGTTCTGAGTGCTAAG
Sqstm1	ATGTGGAACATGGAGGGAAGA	GGAGTTCACCTGTAGATGGGT
Tfam	CCTTCGATTTTCCACAGAACA	GCTCACAGCTTCTTTGTATGCTT
Ucp1	CACCTTCCCGCTGGACACT	CCCTAGGACACCTTTATACCTAATGG
Ulk2	AGCTTCAGCATGAAAACATCGT	CGATTGGCATAAGACAACAGGA
Uvrag	GACTTTGGAATAATGCCGGATCG	CAGCCCATCCAGGTAGACTTT
Wipi1	GCGCTCCGAGGGGAAGTTAT	CCCTTCTGACTTCCACGGCA

SUPPLEMENTARY TABLE LEGENDS

Table S1: Supplementary to Figure 3.
Cluster 1 gene list and associated membership values.

Table S2: Supplementary to Figure 5.
Oligonucleotide sequences of qRT-PCR primers.